

---

# Coupling in Networks of Neuronal Oscillators

Carter Johnson

June 15, 2015

# 1 Introduction

Oscillators are ubiquitous in nature. From the pacemaker cells that keep our hearts beating to the predator-prey population interactions of wild animals, oscillators drive the natural world as we know it. An oscillator is any system that goes through various states cyclically and exhibits periodic behavior. Classic examples are pendulums, springs, and swing sets, but these are small, isolated, and generally inconsequential objects. The Earth, on the other hand, is a very significant oscillator that orbits the sun in a repeating pattern with a “characteristic period” of one year. For an expository introduction to oscillators in the natural world, see [14].

It is simpler mathematically to characterize an oscillator not by its position in physical time or space, but by its position, or “phase”, in its periodic cycle. Mathematicians call this the “phase space” of the oscillator, but it is really less abstract than it sounds. In fact, you already chronicle your life in a phase space— the calendar year! Our calendars don’t really mark our place in time (since who knows when time even began), but they refer to the position of the Earth in its periodic orbit about the sun. It is a convenient convention that does away with the details that may be quite difficult to determine, like the galactic coordinates of our planet or our actual place in the lifetime of the universe.

Many oscillators tend to trace out a single pattern in phase space. While the Earth could orbit the sun in a different pattern, such as Venus’ or Mars’, its current orbit is ideal for life. If a doomsday asteroid knocked the Earth slightly off track, wouldn’t it be great if the Earth had a natural tendency to fall back into the characteristic orbit that we know and love? Oscillators that do just this — return to a particular periodic pattern after a small perturbation — are said to have a “characteristic amplitude” in phase space.

Oscillators can affect each other’s position in phase space through various physical mechanisms and “couple” their periodic behaviors. When you were a kid on the swing sets with a friend, didn’t you notice it was easiest to swing if you hit the peaks exactly when your friend did? Either they were right there beside you — in which case your swings were “in phase” — or at the opposite peak — “in anti-phase”. These two kinds of synchrony are generated by the “coupling effect” of the vibrations through the swing set from one swing to the other. With each pump of your legs, you sent weak vibrations through the swing set that affected the pace of your friend’s swing and slightly changed its phase in its cycle. Eventually, each of your swings’ effects on the other balanced out and the swings fell into synchrony. Depending on how the two of you started swinging, i.e., the initial “phase difference” between your swings, the two of you would swing either in phase or in anti-phase. Determining the eventual synchronous state of such a network of oscillators becomes quite involved when looking at three, four, or even hundreds of oscillators. This analysis becomes even harder as more and more complicated coupling mechanisms are considered.

## The Problem

Neurons are the basic cellular oscillator in central nervous systems like the human brain. A neuron's activity is dominated by the electrical field across its membrane that is generated by ionic currents. A neuron oscillates through oscillations in its electrical field, and at a point in this cycle it releases an electrochemical signal to connected neurons. The phase space of the neuron describes how close the neuron is to firing this signal, and this cycle has both a characteristic period and an amplitude. This means that the oscillations will remain near a constant frequency even when the neuron is perturbed; the neuron acts like our hypothetical fantasy where the Earth is hit by an asteroid but still returns to its life-harboring orbit. For a thorough explanation of the biophysics behind a neuron's periodic activity, see [2].

Neural populations consist of thousands of individual neurons linked together through direct "synaptic" connections. The electrochemical signal sent through the synaptic connections instructs the connected neurons to change their behavior in a way that effectively alters the phase of the connected neurons and brings them closer or further away from firing their own signals. The culmination of these phase-shifting effects through "synaptic coupling" is often network-wide synchronization of firing patterns. This is to say that the timings between one neuron's firing and another's are fixed, and the neurons act like a group of kids swinging together in some fixed, coordinated pattern on the swing set. Again, [2] describes the nature of how synaptic signals affect the electrical dynamics of the connected neurons.

Different synaptic coupling mechanisms and the structure of how neurons are connected in a network gives rise to a multitude of synchronized behaviors. How these many different patterns come to fruition is an ongoing research question. In Part I of this paper, we will introduce the reader to the techniques used in approaching this question. We explain and apply the theory of weakly coupled oscillators and phase response curves to analyze some basic oscillator networks. In Part II, we use the same techniques to explore the effects of delayed negative feedback on oscillator networks.

## History

The biophysics behind the action-potential cycle of a neuron were first described mathematically by Hodgkin and Huxley in their 1952 Nobel-prize winning paper [4], and were greatly simplified in 1981 by Morris and Lecar in [10]. The Morris-Lecar model neuron is an oscillator whose phase space is much more accessible to analytical techniques from nonlinear differential equations than the Hodgkin-Huxley model neuron. In particular, through phase plane analysis the model's characteristic period and amplitude can be found and much can be inferred about the nature of the oscillating neuron. To analyze the effects of delays in oscillator dynamics in Part II, we use a discontinuous model - the Leaky Integrate-and-Fire (LIF) neuron. This model simplifies the dynamics even more to a growth equation

and a fixed reset condition.

Researchers have developed a mathematically rigorous approach to the question of how synaptic coupling gives rise to synchronized firing patterns in networks of neurons, see [15] for an example. The basic idea is to develop a “phase model” for the network of neurons that describes the phases of each neuron in its firing cycle relative to the others, thus simplifying the complicated biophysics into a coupled oscillator problem. To create the phase model, they first determine the characteristic periods and amplitudes of the model neurons. Then experimentally or analytically, a “phase response curve” (PRC) is found that describes how perturbations shift a neuron’s phase closer towards or further away from its firing threshold. The PRC can be used to predict the effects of another neuron’s synaptic input on its firing cycle. Then the biophysics of the synaptic connections are modeled via an interaction function, and the PRC and interaction function together describe each neuron’s phase response to each other’s synaptic input. The steady states of the phase model correspond to synchronized neural network behavior, and we can examine how varying parameters causes qualitative changes in the steady states of the phase model and thus examine how different patterns of neural synchrony are formed.

## Who cares?

Synchronizing oscillations is a hallmark in networks of neurons in the brain and other neural systems [11]. The timings of oscillating neurons in a network determine macro-level behavior. For instance, the running patterns of various mammals correspond directly to different modes of a four-oscillator system which is thought to embody the neural mechanism behind the behavior [13]. In a horse’s gallop, the forward legs move in unison and then the back legs move together at the next step- its forward “oscillators” are in phase with one another and in anti phase with the two back legs. A horse also trots with a similar type of leg-coupling, but its front-left and back-right legs move in unison and then a half-step later its front-right and back-left legs move in unison. An elephant ambles with each foot in turn with a 1/4-step delay between each foot, and a gazelle leaps with all legs at the same time. How the same four-oscillator system gives rise to four distinct patterns is a question about oscillator timings and cellular parameters. This type of neural synchrony has also been shown to be important for many neural functions besides motor behavior, including the *magnum opus* of cognition [11, 8]. In finding out how different timings between oscillating neurons arise, researchers help provide a fuller picture of how neural parameters affect observable behavior.

---

# Part I - Coupling in Morris-Lecar Neurons

## 2 Summary

The goal of this paper is to determine the timing of a Morris-Lecar model neuron's oscillations relative to the timing of periodic input. We create a phase model for a single Morris-Lecar model neuron that describes how a coupled neuron moves about its natural cycle in phase space as opposed to explicitly describing the oscillations of cellular parameters, much like how we describe the Earth's motion about the sun by the calendar year as opposed to the Earth's physical position about the sun. We will derive an ordinary differential equation that describes the rate of change of the phase of the Morris-Lecar oscillator in its periodic "limit cycle" relative to the phase of an external, periodic stimulus. The first periodic input we will consider is just a simple injected sinusoidal current, but we will show how to consider periodic input from another Morris-Lecar neuron. We will extend the phase model to analyze the relative phases between any number of coupled neurons.

We will consider the Morris-Lecar model as our neural oscillator. This neuron's oscillations are described by a system of ordinary differential equations (ODEs). To determine the characteristic period and amplitude of the oscillator, we will use Euler's method (on MATLAB) on the ODE system to iterate through the oscillator's states and find the "limit cycle" of the system. The "limit cycle" is the periodic solution to the differential equations, or the cyclical pattern of states that the oscillator approaches as we run forwards in time.

We must also define "phase" on or near the limit cycle, so that we can be clear about what the phase model is even describing. Next, we derive the "phase response" function  $Z(t)$  of the neuron: how many phases the neuron is shifted about its limit cycle after a small perturbation to its steady oscillations. We use the "adjoint method" (see [12]) to determine this. We then determine an interaction function  $G(X, t)$  that describes the effects on the neuron by the periodic input. We will then combine the phase response and interaction functions to create the phase model.

We will use a convolution integral (in accordance with Malkin Theorem for Weakly Coupled Oscillators) of the interaction function with the PRC to combine the perturbations that the forcing field has on the neuron's oscillations (the interaction function) with the response of the oscillator to external perturbations (the iPRC). This integral sums up the cell's phase response to the ephaptic input and describes the phase evolution of the cell. This creates the phase model — an ODE that describes the oscillator's phase in its cycle relative to the phase of the stimulus. By analyzing the steady states of the phase model, we will describe the phase-locking behavior of the oscillator with the oscillating field. This gives us a clear picture of how the neuron's oscillations are timed with the periodic input.

### 3 Technical Details

#### The Limit Cycle of the Morris-Lecar Model

The Morris-Lecar model describes the electrical dynamics of an oscillating neuron by

$$C \frac{dV}{dt} = -g_{Ca} M_{ss}(V)(V - V_{Ca}) - g_K W(V - V_K) - g_L(V - V_L) + I_{app} \quad (1)$$

$$\frac{dW}{dt} = \phi(W_{ss}(V) - W)/\tau. \quad (2)$$

Where

$$M_{ss}(V) = \left(1 + \tanh\left(\frac{V - V_1}{V_2}\right)\right)/2 \quad (3)$$

$$W_{ss}(V) = \left(1 + \tanh\left(\frac{V - V_3}{V_4}\right)\right)/2. \quad (4)$$

In each of these equations, all the parameters have been nondimensionalized. Equation (1) is a current balance equation for the cellular membrane potential.  $V$  is the cellular membrane potential, and  $C$  is the membrane capacitance. (1) balances an applied current  $I_{app}$  with three ionic currents:  $I_{Ca}$  - the excitatory Calcium ion current,  $I_K$  - the recovery Potassium ion current, and  $I_L$  - the equilibrating leakage current. The  $g_i$  and  $V_i$  are the conductances (or magnitudes) and equilibrium potentials of their respective ionic currents.  $M_{ss}(V)$  is a probability distribution function describing the chance that a number of Calcium ion channels will be open.

Equation (2) describes the recovery dynamics of the cell, and it dominates after the cell sends its signal. Specifically,  $W$  is the normalized Potassium ion conductance.  $\phi$  and  $\tau$  are time constants for the opening and closing of the Potassium ion channels, and  $W_{ss}(V)$  is a probability distribution function of open Potassium channels.

Equation (3),  $M_{ss}(V)$ , is the probability distribution function of open Calcium ion channels, with  $V_1$  as another voltage threshold and  $V_2$  as a voltage normalizer. Equation (4),  $W_{ss}(V)$ , is the probability distribution function of open Potassium ion channels, with  $V_3$  as another voltage threshold and  $V_4$  as a voltage normalizer.

The solution to this system of ordinary differential equations for particular parameter sets is a stable limit cycle. We use the parameter values from figures 8.6 and 8.7 in [10] because they yield a stable limit cycle solution to (1-2):

$$P_1 = \{C = 20; g_{Ca} = 4.4; V_{Ca} = 120; g_K = 8; V_K = -84; g_L = 2; V_L = -60; V_1 = -1.2; V_2 = 18; V_3 = 2; V_4 = 30; \phi = 0.04; \tau = 0.8; \}.$$

By setting  $dV/dt = dW/dt = 0$  (equations (1-2)), we can plot the nullclines to observe that the system has a limit cycle solution.

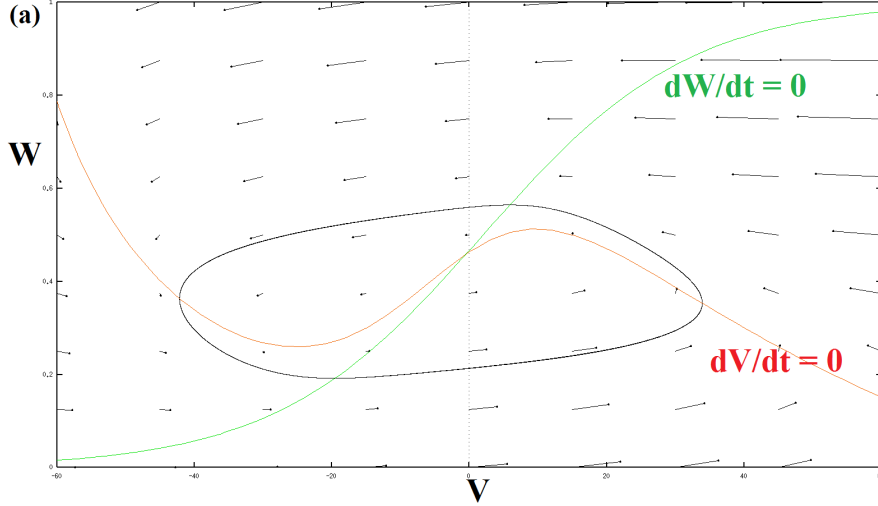


Figure 1: (a) Setting  $dV/dt = dW/dt = 0$  and evaluating the vectors  $(dV/dt, dW/dt)$  at various points, the nullclines and gradient vector field show that the system has a limit cycle solution.

To see this, we first note that the intersection of the nullclines corresponds to a fixed point of the system since  $dV/dt = dW/dt = 0$  means the system is not changing, but the stability of this fixed point is unclear. We evaluate (1) and (2) at points in the  $V - W$  “phase plane” to generate a gradient vector field about the nullclines that describes the directions in which the system is changing at the given points. The vectors right around the fixed point are oriented outwards away from the fixed point, so the fixed point is unstable because small perturbations from the fixed point will cause the system to move away from it. The vectors point inwards around a region encircling the fixed point, so by the Poincare-Bendixson theorem there must be a stable limit cycle solution, since there should be some closed curve that the vectors point along as they switch from pointing inwards to pointing outwards (from the fixed point). Using the dynamical system computing software XPP, we verify that there is indeed a stable limit cycle solution for this parameter set.

For brevity of notation, we let  $X = (V, W)$  and let equations (1-2) be represented in vector form:  $\frac{dX}{dt} = F(X)$ . We use Euler’s method in MATLAB on the ODE system (1-2) to numerically compute the values  $V$  and  $W$  along the trajectory of the system from the initial condition  $V = -40, W = 0$  through the limit cycle. We search the trajectory values to determine the vector  $X_{LC}$  of values  $X = (V, W)$  along the limit cycle.

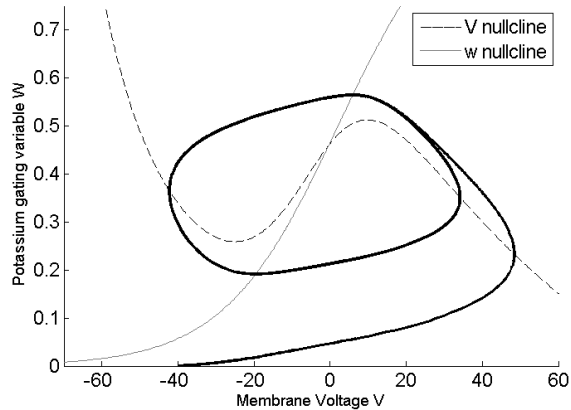


Figure 2: The trajectory of the system in V-W phase space according to (1-4) with initial condition  $V = -40$ ,  $W = 0$ . Computed numerically with Euler’s method in MATLAB with parameter set  $P_1$ .

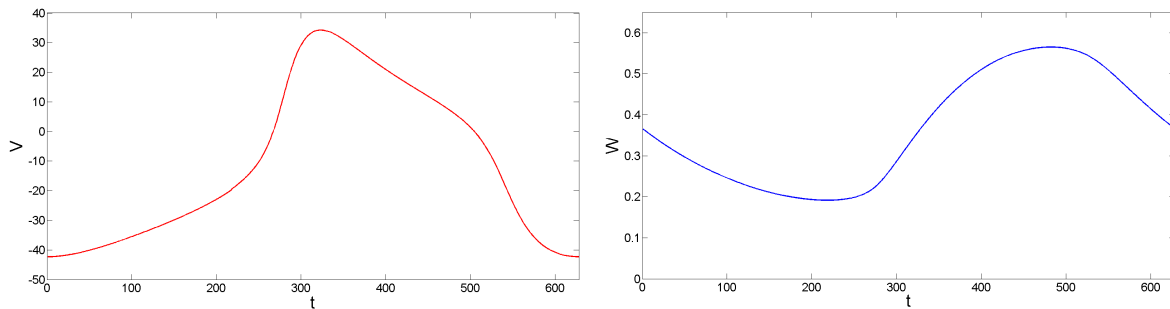


Figure 3: (L) The limit cycle solution to eqns. (1-2) for the cellular membrane potential  $V$ . Computed numerically from Fig. 2 via a search routine. (R) The limit cycle solution to eqns. (1-2) for the recovery variable  $W$ . Computed numerically from Fig. 2 via a search routine.

## Defining Phase on and near the Limit Cycle

We want to clearly define the “phase” of the neuron on or near its limit cycle before we can begin to define a neuron’s “phase response” to input or “phase-locking” in a pair of neurons.

The limit cycle solution to equations (1-2) has some period  $T$ , so we define the phase of the neuron along its limit cycle as

$$\theta(t) = (t + \phi) \bmod T,$$

where the relative phase  $\phi$  is a constant that is determined by where on the limit cycle the neuron begins. The position of the neuron in phase space,  $X(t) = X_{LC}(\theta(t))$ , is given in a one-to-one fashion by the phase, so each point on the limit cycle corresponds to a unique phase  $\theta = X_{LC}^{-1}(X) = \Phi(X)$ .

The limit cycle of the Morris-Lecar model neuron is stable, so every point in phase space, if given as an initial condition to (1-2), will converge to the limit cycle as time goes to infinity. We can extend the domain of  $\Phi(X)$  to points off of the limit cycle by defining the “asymptotic phase” of a point as the phase of another point on the limit cycle whose trajectory coincides with the approaching trajectory as time goes to infinity. This means that for points on the limit cycle, the asymptotic phase is the same as phase, but for points off the limit cycle, we must match trajectories to a point on the limit cycle:

If  $X_0$  is a point on the limit cycle in phase space and  $Y_0$  is a point off the limit cycle, then  $Y_0$  has the same asymptotic phase as  $X_0$  if the solution to (1-2) with initial condition  $Y_0$  converges to the solution to (1-2) with initial condition  $X_0$  as time goes to infinity. We say that  $\Phi(Y) = \Phi(X)$ .

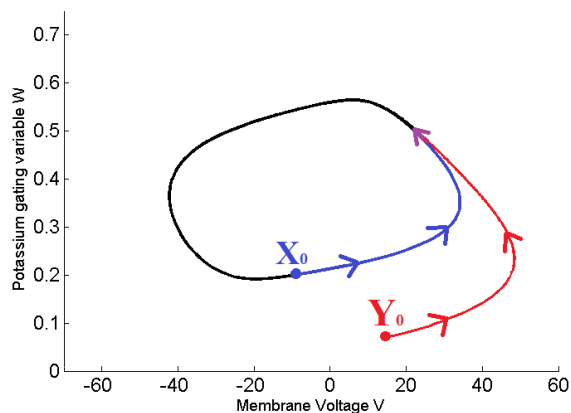


Figure 4:  $X_0$  is a point on the limit cycle in phase space and  $Y_0$  is a point off the limit cycle.  $Y_0$  has the same asymptotic phase as  $X_0$ , i.e.,  $\Phi(Y) = \Phi(X)$ .

## The Infinitesimal Phase Response Curve

Here, we derive the “phase response” of a neuron’s oscillations to external input. When the neuron receives input, it is bumped off its limit cycle to some other point in phase space. But as we saw in the previous section, points off the limit cycle will converge to the limit cycle as time goes to infinity, so we can look at the asymptotic phase of this new position. The difference between this new asymptotic phase and the old asymptotic phase (or rather phase, since it was on the limit cycle) is called the “phase shift”. We quantify these phase shifts in the infinitesimal phase response curve (iPRC). The iPRC is a periodic

function  $Z(t)$  that measures the shift in the asymptotic phase of the neuron in response to infinitesimally small and instantaneous perturbations as a function of where in the limit cycle the neuron was when it was perturbed.

To derive the iPRC, note that the unit along the limit cycle of the oscillator is phase, so the rate of change of phase in time  $\frac{d\theta}{dt} = 1$ . By differentiating  $\theta = \Phi(X)$ , we get

$$\frac{d\theta}{dt} = \nabla_X \Phi(X_{\text{LC}}(t)) \cdot F(X_{\text{LC}}(t)) = 1 \quad (5)$$

where  $\nabla_X \Phi$  is the gradient of  $\Phi(X)$ .

The iPRC measures the oscillator's phase shift in response to small perturbations, so it is defined as the gradient of the phase map  $\nabla_X \Phi(X_{\text{LC}}(t))$ . To see this, suppose an oscillator on its limit cycle at  $X(t) = X_{\text{LC}}(\theta^*)$  with phase  $\theta^* = \Phi(X(t))$  is perturbed by  $\varepsilon U$ , where  $\varepsilon \ll 1$  is a magnitude and  $U$  is a unit vector in some direction in phase space.

Now the neuron is at the state  $X_{\text{LC}}(\theta^*) + \varepsilon U$  with *asymptotic* phase  $\tilde{\theta} = \Phi(X_{\text{LC}}(\theta^*) + \varepsilon U)$ . Using Taylor series,

$$\tilde{\theta} = \Phi(X_{\text{LC}}(\theta^*) + \varepsilon U) = \Phi(X_{\text{LC}}(\theta^*)) + \nabla_X \Phi(X_{\text{LC}}(\theta^*)) (\varepsilon U) + \mathcal{O}(\varepsilon^2). \quad (6)$$

Since  $\varepsilon \ll 1$ , we can ignore the remainder  $\mathcal{O}(\varepsilon^2)$ . Then the phase shift of the oscillator is

$$\Delta\phi(\theta^*) = \Phi(X_{\text{LC}}(\theta^*) + \varepsilon U) - \Phi(X_{\text{LC}}(\theta^*)) = \nabla_X \Phi(X_{\text{LC}}(\theta^*)) \cdot (\varepsilon U).$$

So the phase shift is a function of the phase  $\theta^*$  at which it was perturbed. If we normalize by the strength of the perturbation, we get that  $\Delta\phi(\theta^*)/\varepsilon = \nabla_X \Phi(X_{\text{LC}}(\theta^*)) \cdot U$ .

Thus the gradient of the asymptotic phase map along the limit cycle of the oscillator is the iPRC. It quantifies the phase shift of the oscillator due to weak, brief perturbations at any phase (or asymptotic phase) along the limit cycle.

In practice, however, this derivation of the iPRC yields little to no computational value. There is an alternate derivation, however, that gives us a straightforward numerical method to compute the iPRC. This method is called the adjoint method, and requires that we first introduce the Theory of Weakly Coupled Oscillators.

## The Theory of Weakly Coupled Oscillators

To show that the iPRC can be found via the adjoint method, we must introduce some more theory. Fortunately, this theory also gives us a direct way to use the iPRC  $Z(t)$  and the interaction function  $G(X, t)$  to derive the phase model of our system. It is the intermediate step between the unperturbed neural behavior and the coupled neural behavior.

We consider our coupled Morris-Lecar model neuron. Let  $X = (V, W)$  be the cellular membrane potential and recovery variable for the *uncoupled* neuron, so that  $\frac{dX}{dt} = F(X)$

is the *uncoupled* ODE system as in (1-2). Let  $G(X, t)$  be the interaction function for the neuron with the periodic input; we will derive this soon. Then the ODE for the *coupled* Morris-Lecar neuron's oscillations is

$$\frac{dX}{dt} = F(X) + \varepsilon G(X, t),$$

where  $\varepsilon \ll 1$  since coupling is understood to be weak relative to the intrinsic dynamics of the neuron  $F(X)$ .

We are interested in the difference between the phase of the neuron in its oscillations and the phase of the oscillating forcing field, and how this “relative phase” difference changes over time as the neuron is periodically perturbed. We want to construct a phase model — an ODE that describes not the electrochemical states of the neuron but simply the relative phase of the neuron in its limit cycle. The phase model will describe how the neuron's limit cycle *timing* is shifted as a result of the perturbations, and the steady states of the phase model will correspond to relative phase differences between the neuron and the periodic input that do not change over time. Constant relative phase differences describe how the neuron's oscillations are timed with respect to the timing of the stimulus.

The Malkin Theorem for Weakly Coupled Oscillators (see [5]) shows us how to derive a phase model for our system and yields a method of finding the infinitesimal phase response curve (iPRC).

### Malkin Theorem for Weakly Coupled Oscillators

Consider a weakly coupled oscillator of the form

$$\frac{dX}{dt} = F(X) + \varepsilon G(X, t),$$

that has an asymptotically stable  $T$ -periodic solution  $X_{\text{LC}}$  when uncoupled (i.e., with interaction function  $G(X, t) = 0$ ).

Let  $\tau = \varepsilon t$  be slow time and let  $\phi(\tau) \in [0, T]$  be the phase shift away from the natural oscillation  $X_{\text{LC}}(t)$  (also in  $[0, T]$ ) that results from the coupling effects  $\varepsilon G(X, t)$ .

Then,  $\phi \in [0, T]$  is a solution to

$$\frac{d\phi}{d\tau} = \frac{1}{T} \int_0^T Z(t + \phi) \cdot G(X_{\text{LC}}(t + \phi), t) dt,$$

where  $Z(t)$  is the unique nontrivial  $T$ -periodic solution to the *adjoint* linear system

$$\frac{dZ}{dt} = -[DF(X_{\text{LC}}(t))]^T Z \tag{7}$$

satisfying the normalization condition

$$Z(0) \cdot F(X_{\text{LC}}(0)) = 1, \tag{8}$$

and where  $DF(X_{\text{LC}}(t))$  is the Jacobian of partial derivatives of the vector function  $F(X)$  evaluated along the limit cycle  $X_{\text{LC}}(t)$ .

We have already computed the limit cycle  $X_{\text{LC}}$  in the previous subsection, but we're still missing  $Z(t)$  and  $G(X)$ . We will derive the  $T$ -periodic function  $Z(t)$ , which coincides with the infinitesimal phase response curve (the iPRC). We will prove that  $Z(t)$  is exactly the iPRC of the neuron by showing that  $\nabla_X \Phi(X_{\text{LC}}(t))$  satisfies the adjoint equation (7) and the normalization condition (8) in Malkin Theorem.

**Theorem** The iPRC  $\nabla_X \Phi(X_{\text{LC}}(t))$  satisfies

$$\frac{d}{dt} \nabla_X \Phi(X_{\text{LC}}(t)) = -[DF(X_{\text{LC}}(t))]^T \nabla_X \Phi(X_{\text{LC}}(t)) \quad (9)$$

and

$$\nabla_X \Phi(X_{\text{LC}}(0)) \cdot F(X_{\text{LC}}(0)) = 1. \quad (10)$$

*Proof.* Consider two solutions to the system (1-2):

$X(t) = X_{\text{LC}}(t + \phi)$  and  $Y(t) = X_{\text{LC}}(t + \phi) + p(t)$ , where  $p(t)$  is the trajectory back onto the limit cycle from a small perturbation  $p(0) \ll 1$ .  $X(t)$  starts on the limit cycle at  $X(0) = X_{\text{LC}}(\phi)$ , while  $Y(t)$  starts just off the limit cycle at  $Y(0) = X_{\text{LC}}(\phi) + p(0)$ . The initial perturbation  $p(0)$  is small and the limit cycle is stable, so  $Y(t)$  approaches  $X_{\text{LC}}(t + \phi_2)$ , where  $\phi_2 \neq \phi$ .

Thus  $p(t)$  remains small (i.e.,  $|p| \ll 1$ ) and since  $Y(t)$  remains close to the limit cycle,

$$\begin{aligned} \frac{dX_{\text{LC}}(t)}{dt} + \frac{dp}{dt} &= \frac{dY}{dt} = F(Y(t)) \\ F(X_{\text{LC}}(t)) + \frac{dp}{dt} &= F(X_{\text{LC}}(t) + p(t)) \end{aligned}$$

and by Taylor Series, we can expand  $F(X_{\text{LC}}(t) + p(t))$  so that

$$F(X_{\text{LC}}(t)) + \frac{dp}{dt} = F(X_{\text{LC}}(t)) + DF(X_{\text{LC}}(t)) \cdot p(t) + \mathcal{O}(|p|^2),$$

where  $DF(X_{\text{LC}}(t))$  is the Jacobian matrix of partial derivatives of the vector function  $F(X)$  evaluated along the limit cycle  $X_{\text{LC}}(t)$ . Since  $|p| \ll 1$ , we can ignore the  $\mathcal{O}(|p|^2)$  term and thus  $p(t)$  satisfies  $\frac{dp}{dt} = DF(X_{\text{LC}}(t)) \cdot p(t)$ .

The phase difference between the two solutions is

$$\Delta\phi = \Phi(X_{\text{LC}}(t + \phi) + p(t)) - \Phi(X_{\text{LC}}(t + \phi)) = \nabla_X \Phi(X_{\text{LC}}(t + \phi)) \cdot p(t) + \mathcal{O}(|p|^2), \quad (11)$$

where the last equality holds by our derivation for the iPRC.

The two solutions continue as time goes to infinity without any further perturbations, so the phase difference has no impetus to change. The asymptotic phases of these solutions evolve in time as the solutions travel about the limit cycle, but the phase difference between them,  $\Delta\phi$ , remains constant. Taking the derivative of (11),

$$\begin{aligned} 0 &= \frac{d}{dt}(\nabla_X \Phi(X_{\text{LC}}(t + \phi)) \cdot p(t)) \\ &= \frac{d}{dt}(\nabla_X \Phi(X_{\text{LC}}(t + \phi))) \cdot p(t) + \nabla_X \Phi(X_{\text{LC}}(t + \phi)) \cdot \frac{dp}{dt} \\ &= \left( \frac{d}{dt}(\nabla_X \Phi(X_{\text{LC}}(t + \phi))) + DF(X_{\text{LC}}(t + \phi))^T(\nabla_X \Phi(X_{\text{LC}}(t + \phi))) \right) \cdot p(t) \end{aligned}$$

This holds for any arbitrarily small perturbation  $p(t)$  in any direction in phase space, so we have that

$$\frac{d}{dt}(\nabla_X \Phi(X_{\text{LC}}(t + \phi))) = -DF(X_{\text{LC}}(t + \phi))^T(\nabla_X \Phi(X_{\text{LC}}(t + \phi))). \quad (12)$$

Hence  $\nabla_X \Phi(X_{\text{LC}}(t))$  satisfies the adjoint equation (9). The normalization condition (10) is satisfied by the definition of the phase map since  $\frac{d\phi}{dt} = \nabla_X \Phi(X_{\text{LC}}(t)) \cdot X'_{\text{LC}}(t) = 1$ .  $\square$

To compute the iPRC  $Z(t)$ , we note that since equation (7) is the adjoint system to the isolated model neuron linearized around its limit cycle, it has the opposite stability of the original system. Thus we integrate equation (7) backwards in time using Euler's method to get the unstable periodic solution. We then normalize the periodic solution by computing  $Z(t) \cdot F(X_{\text{LC}}(t))$  for every  $t \in [0, T]$  and dividing  $Z(t)$  by the average value.

The iPRC  $Z(t)$  measures the response of a Morris-Lecar neuron's oscillations to weak perturbations. It has two components: a voltage response in  $V$ , and a recovery variable response in  $W$ . Each response curve quantifies the amount by which the respective variable will be shifted (the y-axis) following an infinitesimally small, instantaneous perturbation at a particular timing in the limit cycle (the x-axis).

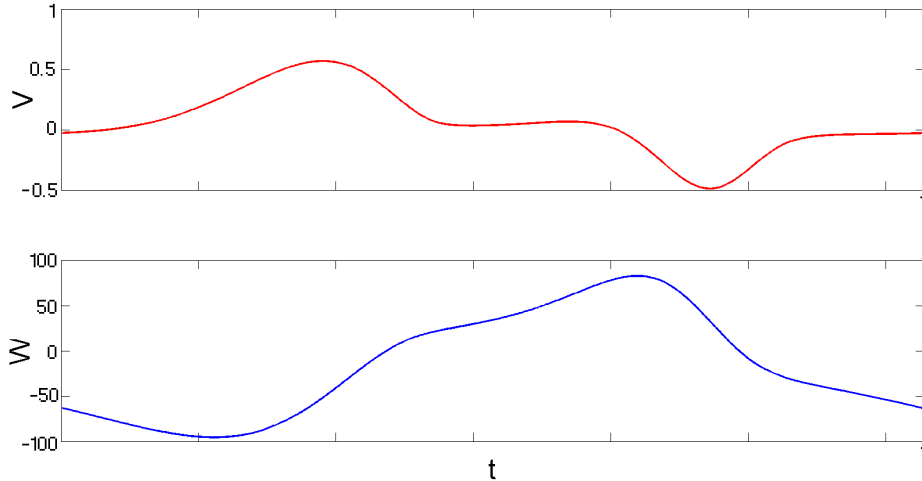


Figure 5: The voltage response component  $V$  and recovery variable component  $W$  of the iPRC  $Z_i(t)$ . Computed in MATLAB using Euler’s method on the adjoint system (7-8) with parameter set  $P_1$ .

## 4 Exploration

Up to this point, we have set up the reader to construct a phase model for the Morris-Lecar neuron coupled with any type of periodic input. We will now consider a sinusoidal current input and show how the phase model can be completed. Then we will show how the phase model can be extended to a network of any number of identical neuronal oscillators, and explore a few simple examples.

We will derive an interaction function  $G(X, t)$  that describes the effects of an periodically injected current on the phase of the Morris-Lecar model neuron. Using Malkin Theorem, we will combine  $G(X, t)$  with the phase response function  $Z(t)$  from last section to create our phase model. We will then examine the steady states of the phase model, which correspond to phase-locked positions of the neuron with respect to the phase of the ephaptic oscillating field. This will yield insight into how a single neuron behaves when periodically perturbed.

We will now explore synaptic coupling in Morris-Lecar neuron pairs gives rise to synchronized firing patterns. We will use the same set-up as the single-cell case: we use the same limit cycle and iPRC for the model neurons and an extended version of the Malkin theorem from Section 3. We use a different interaction function that models an exponentially decaying synapse between the two cells.

We will then explore the example from the end of Section 1: the neural “mechanisms” behind different quadruped gaits. We will show how changing the synaptic coupling between

four Morris-Lecar neurons gives rise to the many different four-oscillator patterns.

## The Single Cell with a Sinusoidal Current Input

Here we derive the interaction function  $G(X, t)$  that describes the sinusoidal input to the Morris-Lecar model neuron and show how the cell phase-locks with the current.

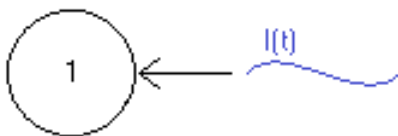


Figure 6: The single cell with sinusoidal input.

The sinusoidal current  $I(t)$  has the same period as the neuron, and it is given by

$$I(t) = A \cdot \sin\left(\frac{2\pi t}{T}\right), \quad (13)$$

where  $A$  is the amplitude of the current and  $T$  is the period of the Morris-Lecar neuron's limit cycle.

Because the current is injected straight across the cellular membrane, the effect on the cell is exactly the sinusoidal current. See [1] for a further exploration of sinusoidal current injections. Thus  $G(X, t) = I(t)$ .

We now finally have all the pieces to create the phase model for the Morris-Lecar model neuron with a sinusoidal current input. We have the limit cycle of the neuron  $X_{LC}(t)$ , the phase response function  $Z(t)$ , and the interaction function  $G(X, t)$ . Referring back to Malkin Theorem for Weakly Coupled Oscillators, we have that the phase shifts  $\phi$  away from the natural oscillations  $X_{LC}(t)$  solve

$$\frac{d\phi}{d\tau} = \frac{1}{T} \int_0^T Z(t) \cdot G(X_{LC}(t), t - \phi) dt = \frac{1}{T} \int_0^T Z(t) \cdot I(t - \phi) dt, \quad (14)$$

We numerically compute the values of equation (14) in  $[0, T]$  using a MATLAB routine. We then search this solution for zeroes, which correspond to fixed phase differences of the system, and align our limit cycle  $X_{LC}$  with the periodic input eqn. (13) at the stable phase difference to illustrate the natural timing of the system.

## The Interaction Function for Synaptic Interactions

Now we want to use our thoroughly examined techniques to explore how phase-locking occurs between any number of Morris-Lecar neurons. We will use a non-summing, exponentially-decaying synapse for the connections between neurons, as in [6]. This type of synaptic input

is modeled via

$$S(t) = \alpha e^{-t/\tau}, \quad (15)$$

where  $\alpha$  is the strength of the synaptic coupling, and  $\tau$  is the synaptic decay rate. We take  $\alpha > 0$  to indicate an excitatory synapse and  $\alpha < 0$  to indicate an inhibitory synapse. Since the magnitude of  $\alpha$  will not affect the phase-locking results, we take  $|\alpha| = 1$ , and we also take  $\tau = 100$  as in [6]. We take our interaction function for effect of input from the  $j^{\text{th}}$  neuron onto the  $i^{\text{th}}$  neuron to be

$$G(X_i, X_j, t) = S(t - \psi_{i,j}),$$

where  $\psi_{i,j} = \phi_j - \phi_i$  is the relative phase difference between the phase  $\phi_i$  of the  $i^{\text{th}}$  neuron in its limit cycle  $X_{\text{LC}}^i$  and the phase  $\phi_j$  of the  $j^{\text{th}}$  neuron in its limit cycle  $X_{\text{LC}}^j$ .

## An Extended Version of Malkin Theorem

We must extend Malkin Theorem from Section 3 to analyze a network of  $n$  coupled, identical Morris-Lecar neurons. See [5] for a full derivation.

### Malkin Theorem for Weakly Coupled Oscillators

Consider a system of weakly coupled oscillators of the form

$$\frac{dX_i}{dt} = F(X_i) + \varepsilon G(X_i, X_j, t), \quad i = 1, \dots, n,$$

where each ODE has an asymptotically stable  $T$ -periodic solution  $X_{\text{LC}}^i$  when uncoupled (i.e., with interaction function  $G(X_i, X_j, t) = 0$ ).

Let  $\tau = \varepsilon t$  be slow time and let  $\phi_i(\tau) \in [0, T]$  be the phase shift of the  $i^{\text{th}}$  neuron away from its limit cycle oscillations  $X_{\text{LC}}^i(t)$  (also in  $[0, T]$ ) that results from the coupling effects  $\varepsilon G(X_i, X_j, t)$ .

Then,  $\phi_i \in [0, T]$  ( $i = 1, \dots, n$ ) is a solution to

$$\frac{d\phi_i}{d\tau} = \frac{1}{T} \int_0^T Z(t) \cdot \sum_{j=1}^n G(X_{\text{LC}}^i(t), X_{\text{LC}}^j(t + \phi_j - \phi_i), t) dt,$$

where  $Z(t)$  is the iPRC for the identical cells.

## The Two-Cell Phase Model

Here we consider a pair of Morris-Lecar model neurons connected together via exponentially decaying synapses. Inhibitory synapses (negative  $\alpha$  in eqn.(15)) will yield antiphase synchrony, while excitatory synapses (positive  $\alpha$ ) will yield in-phase synchrony.

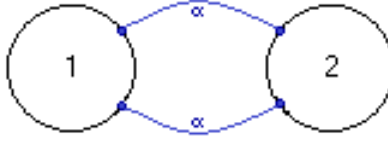


Figure 7: The two-cell network.

We are interested in the difference between the phase of the first neuron in its oscillations and the phase of the second neuron in its oscillations, and how this “relative phase” difference changes over time as the neuron perturb one another. We want to construct a phase model — a pair of ODEs that describe not the electrochemical states of each neuron but simply the relative phases of each neuron in its limit cycle. The phase model will describe how each neuron’s limit cycle *timing* is shifted as a result of the perturbations, and the steady states of the phase model will correspond to relative phase differences between the two neurons that do not change over time. Constant relative phase differences describe how the first neuron’s oscillations are timed with respect to the oscillations of the second neuron.

The Malkin Theorem for Weakly Coupled Oscillators yields the phase model for our two-cell system.

$$\frac{d\phi_i}{d\tau} = \frac{1}{T} \int_0^T Z(t) \cdot \alpha S(t + \phi_j - \phi_i) dt, \quad i, j = 1, 2,$$

We numerically compute the values of the two ODEs in  $[0, T]$  using a MATLAB routine. We then find the evolution of the relative phase *difference*

$$\frac{d\psi}{d\tau} = \frac{d\phi_2}{d\tau} - \frac{d\phi_1}{d\tau}. \quad (16)$$

We then search eqn. (16) for zeroes, which correspond to fixed phase differences of the system, and align the first limit cycle,  $X_{LC}^1$ , with the second limit cycle,  $X_{LC}^2$ , at the stable phase difference to illustrate the natural timing of the system.

## The Four-Cell Phase Model

Here we consider a set of four Morris-Lecar neurons connected together via exponentially decaying synapses.

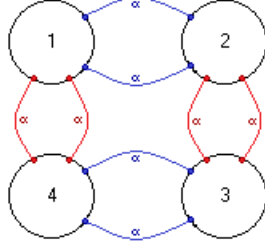


Figure 8: The four-cell network.

The Malkin Theorem for Weakly Coupled Oscillators yields the phase model for our four-cell system.

$$\begin{aligned} \frac{d\phi_1}{d\tau} &= \frac{1}{T} \int_0^T Z(t) \cdot [\alpha_{1,2}S(t + \phi_2 - \phi_1) + \alpha_{1,3}S(t + \phi_3 - \phi_1) + \alpha_{1,4}S(t + \phi_4 - \phi_1)] dt \\ \frac{d\phi_2}{d\tau} &= \frac{1}{T} \int_0^T Z(t) \cdot [\alpha_{1,2}S(t + \phi_1 - \phi_2) + \alpha_{2,3}S(t + \phi_3 - \phi_2) + \alpha_{2,4}S(t + \phi_4 - \phi_2)] dt \\ \frac{d\phi_3}{d\tau} &= \frac{1}{T} \int_0^T Z(t) \cdot [\alpha_{1,3}S(t + \phi_1 - \phi_3) + \alpha_{2,3}S(t + \phi_2 - \phi_3) + \alpha_{3,4}S(t + \phi_4 - \phi_3)] dt \\ \frac{d\phi_4}{d\tau} &= \frac{1}{T} \int_0^T Z(t) \cdot [\alpha_{1,4}S(t + \phi_1 - \phi_4) + \alpha_{2,4}S(t + \phi_2 - \phi_4) + \alpha_{3,4}S(t + \phi_3 - \phi_4)] dt, \end{aligned}$$

The intrepid reader who has made it this far is now probably wondering to himself what sort of foul sorcery must be summoned to analyze this beast of a model. We can examine the symmetry of the network to simplify the problem and find the phase-locked differences between these four cells.

If we take the four cells and split them into two pairs, we can connect each pair with excitatory synapses to induce in-phase synchrony between the two, and then we can connect the two pairs together with inhibitory synapses to induce antiphase synchrony. Setting all  $\alpha_{i,j}$  equal in magnitude, we let  $\alpha_{i,j} > 0$  for excitatorily coupled pairs  $i, j$  and  $\alpha_{i,j} < 0$  for inhibitorily coupled pairs  $i, j$ , the system of relative phase differences  $\frac{d\psi_{i,j}}{d\tau} = \frac{d\phi_j}{d\tau} - \frac{d\phi_i}{d\tau}$  simplifies.

As an example, considered the network where cells 1 and 2 are paired together with excitatory synapses, cells 3 and 4 are paired together with identical excitatory synapses, and the two sets of pairs are coupled together with identical inhibitory synapses between

cells 1 and 4 and between cells 2 and 3. Then the relative phase differences simplify:

$$\begin{aligned}\frac{d\psi_{1,2}}{d\tau} &= \frac{d\phi_2}{d\tau} - \frac{d\phi_1}{d\tau} = \frac{1}{T} \int_0^T Z(t) \cdot [\alpha_{1,2}(S(t + \phi_1 - \phi_2) - S(t + \phi_2 - \phi_1)) \\ &\quad + \alpha_{2,3}S(t + \phi_3 - \phi_2) - \alpha_{1,4}S(t + \phi_4 - \phi_1)] dt \\ \implies \frac{d\psi_{1,2}}{d\tau} &= \frac{1}{T} \int_0^T Z(t) \cdot \alpha_{1,2}[S(t + \phi_1 - \phi_2) - S(t + \phi_2 - \phi_1)] dt,\end{aligned}$$

since  $\alpha_{2,3} = \alpha_{1,4}$  and the convolutions with  $S$  will be the same because of symmetrical behavior.

$$\begin{aligned}\frac{d\psi_{1,4}}{d\tau} &= \frac{d\phi_4}{d\tau} - \frac{d\phi_1}{d\tau} = \frac{1}{T} \int_0^T Z(t) \cdot [\alpha_{1,4}(S(t + \phi_1 - \phi_4) - S(t + \phi_4 - \phi_1)) \\ &\quad + \alpha_{3,4}S(t + \phi_3 - \phi_4) - \alpha_{1,2}S(t + \phi_2 - \phi_1)] dt \\ \implies \frac{d\psi_{1,4}}{d\tau} &= \frac{1}{T} \int_0^T Z(t) \cdot \alpha_{1,4}[S(t + \phi_1 - \phi_4) - S(t + \phi_4 - \phi_1)] dt,\end{aligned}$$

since  $\alpha_{3,4} = \alpha_{1,2}$  and the convolutions with  $S$  will be the same because of symmetrical behavior. Similarly,

$$\frac{d\psi_{1,3}}{d\tau} = \frac{d\phi_3}{d\tau} - \frac{d\phi_1}{d\tau} = \frac{1}{T} \int_0^T Z(t) \cdot \alpha_{1,3}[S(t + \phi_1 - \phi_3) - S(t + \phi_3 - \phi_1)] dt.$$

Each of these ODE's is the same as eqn. (16), albeit with a different sign for  $\alpha$ . Thus cells 1 and 2 are indeed coupled in in-phase synchrony, cells 1 and 4 are coupled in antiphase, cells 1 and 3 are coupled in antiphase. Thus we can infer that cells 3 and 4 are coupled in-phase, that cells 2 and 3 are coupled in antiphase, and that cells 2 and 4 are coupled in antiphase.

Varying the pairings of the four cells, we can obtain any similar pairing pattern — where we have two pairs each in in-phase synchrony but offset from one another. By changing the coupling between the two sets of pairs to excitatory synapses, we will obtain in-phase synchrony between the pairs.

There is one more behavior we can still obtain: a phase difference of  $1/4$  between each cell in a ring. That is to say, for example, that if cell 1 is at phase 0, then cell 2 is at phase  $1/4$ , cell 3 is at phase  $1/2$ , and cell 4 is at phase  $3/4$ . This can be obtained by setting all the  $\alpha$  equal, and whether the synapses are inhibitory or excitatory (i.e., whether  $\alpha$  is positive or negative), we will be able to obtain this phase-locked state.

Consider  $\frac{d\psi_{1,2}}{d\tau}$  with  $\alpha_{i,j} = \alpha$  for all  $i, j$  and with  $\phi_1 = 0, \phi_2 = 1/4, \phi_3 = 1/2, \phi_4 = 3/4$ :

$$\begin{aligned}\frac{d\psi_{1,2}}{d\tau} &= \frac{d\phi_2}{d\tau} - \frac{d\phi_1}{d\tau} = \frac{1}{T} \int_0^T Z(t) \cdot \alpha [S(t + \phi_1 - \phi_2) - S(t + \phi_2 - \phi_1) + S(t + \phi_3 - \phi_2) - S(t + \phi_4 - \phi_1)] dt \\ \frac{d\psi_{1,2}}{d\tau} &= \frac{1}{T} \int_0^T Z(t) \cdot \alpha [S(t - 1/4) - S(t + 1/4) + S(t + 1/4) - S(t + 3/4)] dt \\ \frac{d\psi_{1,2}}{d\tau} &= 0,\end{aligned}$$

where the last equality holds because  $S(t - 1/4) = S(t + 3/4)$  because  $-3/4$  is the same as  $+1/4$  when phase is in  $[0, 1]$ . Thus the pattern of  $1/4$  phase differences between cells in a ring is a possible phase-locked position for a set of 4 Morris-Lecar neurons.

## 5 Results

### The Single Cell with a Sinusoidal Current Input

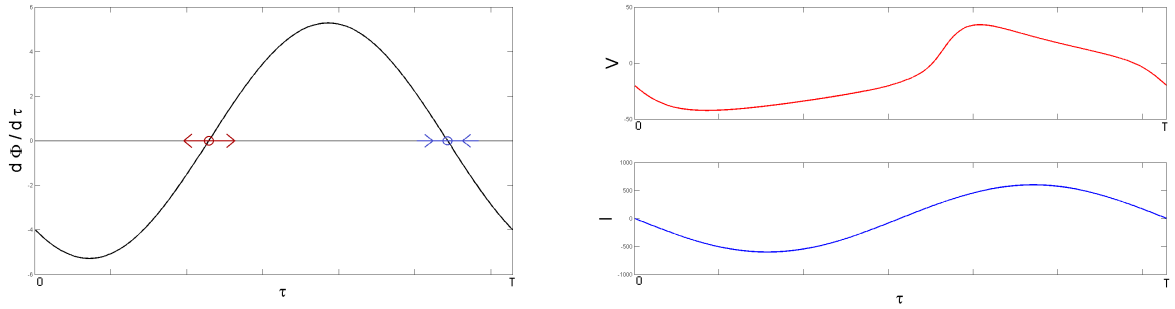


Figure 9: (L) The rate of change of the phase difference between the phase of the Morris-Lecar model neuron and the phase of the sinusoidal input. (R) The oscillations of the Morris-Lecar model neuron timed with the oscillations of the sinusoidal input. One period length shown.

Examining the values of equation (14) in Figure 9, it is clear that the neuron has an unstable phase-locked state  $\psi_1$  around phase 0, and a stable phase-locked state  $\psi_2$  around phase  $1/2$ . To see this, note that  $\frac{d\phi}{dt}$  is positive to the left of phase  $\psi_2$  and negative to the right. Thus, if the phase difference is greater than  $\psi_2$ , it will decrease until it reaches  $\psi_2$ , at which point the rate of change is zero; similarly, if the phase difference is less than  $\psi_2$ , it will increase until it reaches  $\psi_2$ . Analogously, phase  $\psi_1$  has the opposite stability.

## The pair of Morris-Lecar neurons with synaptic connections

### Case 1: Inhibitory Coupling ( $\alpha < 0$ ).

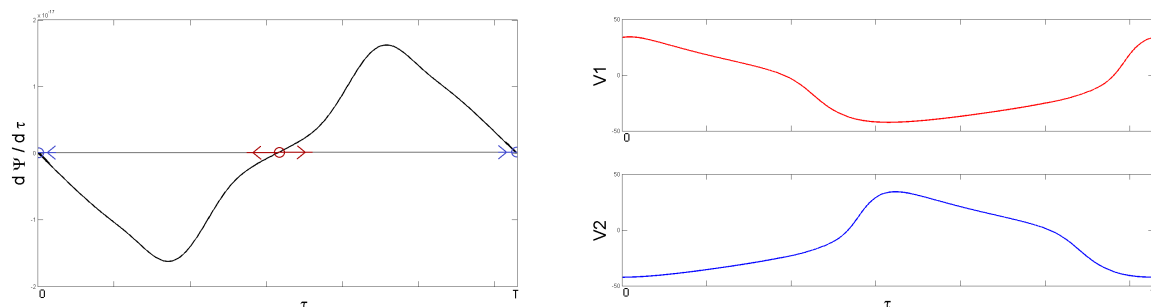


Figure 10: (L) The rate of change of the phase difference between the phases of the two Morris-Lecar model neurons inhibitory coupled. (R) The oscillations of the Morris-Lecar model neuron timed with the oscillations of the second. One period length shown.

Examining the values of equation (14) in Figure 10, it is clear that the neuron has an unstable phase-locked state  $\psi_1$  around phase 0, and a stable phase-locked state  $\psi_2$  around phase 1/2. To see this, note that  $\frac{d\psi}{dt}$  is positive to the left of phase  $\psi_2$  and negative to the right. Thus, if the phase difference is greater than  $\psi_2$ , it will decrease until it reaches  $\psi_2$ , at which point the rate of change is zero; similarly, if the phase difference is less than  $\psi_2$ , it will increase until it reaches  $\psi_2$ . Analogously, phase  $\psi_1$  has the opposite stability.

### Case 2: Excitatory Coupling ( $\alpha > 0$ ).

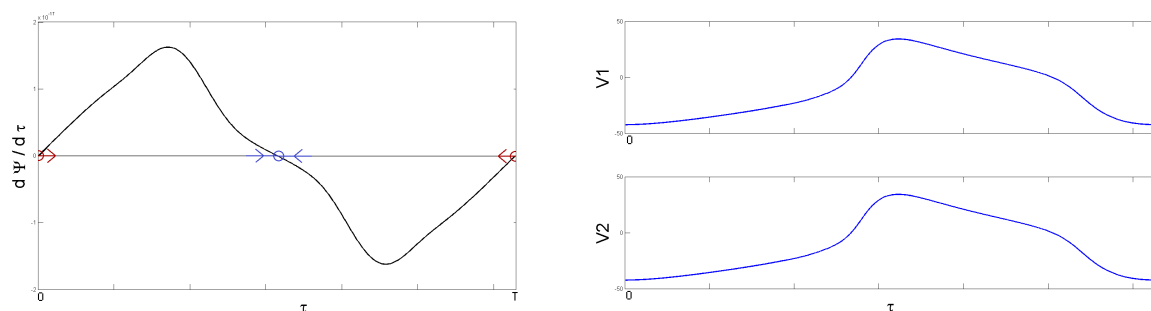


Figure 11: (L) The rate of change of the phase difference between the phases of the two Morris-Lecar model neurons excitatorily coupled. (R) The oscillations of the Morris-Lecar model neuron timed with the oscillations of the second. One period length shown.

Examining the values of equation (14) in Figure 9, it is clear that the neuron has a

stable phase-locked state  $\psi_1$  around phase 0, and a stable phase-locked state  $\psi_2$  around phase  $1/2$ . To see this, note that  $\frac{d\Phi}{dt}$  is positive to the left of phase  $\psi_1$  and negative to the right. Thus, if the phase difference is greater than  $\psi_1$ , it will decrease until it reaches  $\psi_1$ , at which point the rate of change is zero; similarly, if the phase difference is less than  $\psi_1$ , it will increase until it reaches  $\psi_1$ . Analogously, phase  $\psi_2$  has the opposite stability.

## The Four Cell System

### Case 1: Inner-Pair Synchrony, Intra-Pair Antiphase.

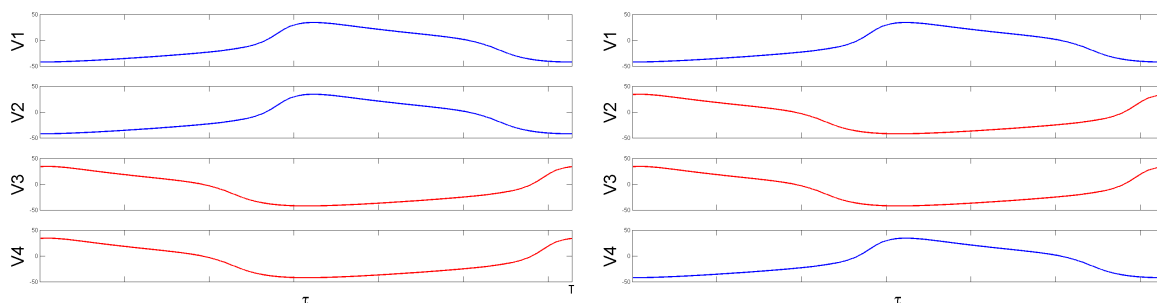


Figure 12: (L) The oscillations of cells 1 and 2 are paired and in antiphase with the paired oscillations of cells 3 and 4. (R) The oscillations of cells 1 and 4 are paired and in antiphase with the paired oscillations of cells 2 and 3. One period length shown.

Here we see how simply changing a few synaptic parameters can make a horse switch from a trot to a gallop. On the right of Figure 12, we have a possible neural mechanism for a horse trot, where legs 1 and 4 (the front left and back right) move together and legs 2 and 3 (the front right and back left) move together a half-step later. On the left of Figure 12, we have a possible neural mechanism for a horse gallop, where legs 1 and 2 (the front legs) move together and legs 3 and 4 (the back legs) move together a half-step later.

### Case 2: Four-Cell In-Phase Synchrony

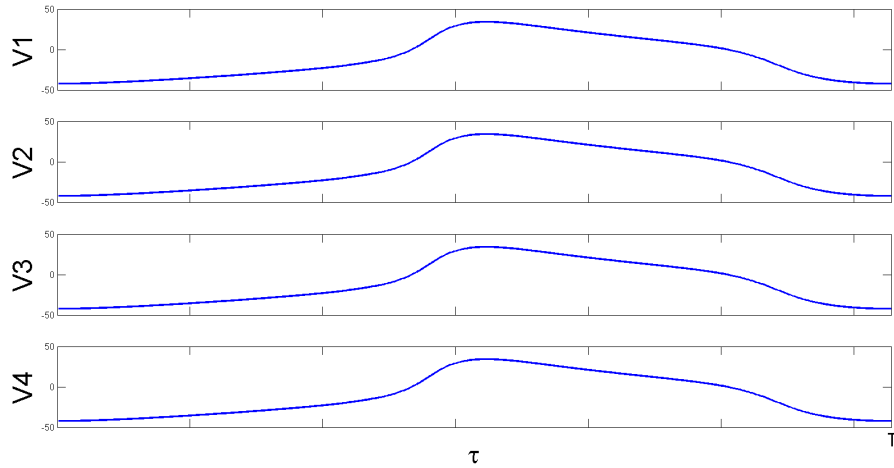


Figure 13: The oscillations of cells 1, 2, 3, and 4 are timed together. One period length shown.

Here we have a possible neural mechanism for a gazelle's leap, where all legs move together at the same time.

**Case 3: Four-Cell 1/4-Phase Synchrony**

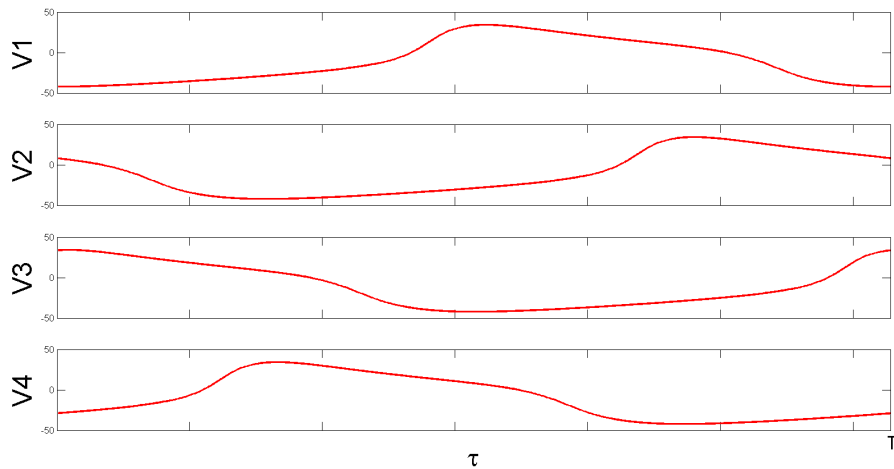


Figure 14: The oscillations of cells 1, 2, 3, and 4 are timed at 1/4 differences together. One period length shown.

Here we have a possible neural mechanism for an elephant's amble, where each leg

moves in turn with a  $1/4$ -step between each movement. Thus the four-cell neural oscillator system is capable of each of the synchronizations mentioned in Section 1, and which pattern the system is in depends entirely on the structure and connectivity of the four neurons.

## 6 Closing Remarks

The possibilities for modeling neural systems are endless now that we have been caught up to speed on how to derive the phase model for the Morris-Lecar neurons. In fact, one can extend our derivation to any other neural model, or even any sort of model with a periodic solution. One can vary the connections between neurons, the structure of the neural network, and even the neural parameters themselves to study almost any observable behavior. Varying the parameters of individual neurons throughout the system allows one to study the effects of heterogeneity on neural behavior, while varying the synaptic connection parameters between neurons throughout the system is another way to study these same effects. One can study even further the effects of differing input to single neurons, and still more work can be done to study alternative connection mechanisms such as ephaptic coupling in neural networks. In Part II, we will explore the effects of adding neural delays to the individual neuron and to the system of neurons.

---

# Part II - Phase Response Properties and Phase-Locking in Neural Systems with Delayed Negative-Feedback

## 7 Introduction

Synchronous activity is a hallmark in networks of neurons in the brain and other neural systems. This synchrony is often associated with oscillatory behavior [11] and has been shown to be important for a multitude of neural functions, including motor behavior and cognition [11, 8]. Coordinated oscillations arise from the combination of intrinsic properties of neurons, synaptic coupling between neurons, and indirect or direct synaptic feedback to a neuron. Synchronous activity (sometimes with nonzero phase lag) occurs despite the inherent delays in synaptic communication pathways between neurons [8]. These delays arise from conduction delays in dendrites and axons, synaptic kinetics, and polysynaptic pathways [9, 7, 3].

Here we use an idealized model to examine how synaptic delays in feedback pathways shape the properties of the oscillatory activity, including the period and the response to external input, and also how delays in synaptic coupling between cells affect synchronization. The model neuron we examine is a leaky integrate-and-fire (LIF) neuron that has an applied constant current and a self-inhibiting synapse with a delay, which we call the Delayed Self-Inhibition (DSI) Cell. This simple model captures the qualitative behavior of simple neuron populations with delayed negative-feedback mechanisms.

We first determine how the DSI cell's characteristic period depends on cellular and synaptic feedback parameters. We then quantify the cell's phase response to perturbations at various phases in its cycle, defining the infinitesimal phase response curve (iPRC). The iPRC is then used along with the theory of weak coupling [12] to analyze interactions between a pair of DSI cells. We couple two DSI cells together via inhibitory synapses with delays, and model the evolution of the phase difference between the two cells. We then examine the effect of varying the synaptic delay between the two cells and describe the bifurcations that occur in the phase-locking behavior of the two-cell system.

## 8 The Delayed Self-Inhibitory (DSI) Cell

The standard Leaky Integrate-and-Fire (LIF) model idealizes the electrical dynamics of a neuron by including only a leakage current and a bias current  $I$  in the subthreshold dynamics and reducing the action potential (or spike) to a single spike-reset condition. With all variables and parameters nondimensionalized, the cell's membrane potential  $V$

evolves according to the differential equation

$$\frac{dV}{dt} = -V + I. \quad (17)$$

When the membrane potential hits the firing threshold at  $V = 1$ , the cell "fires" a spike and the membrane potential is reset to  $V = 0$ , i.e.,

$$V(t^-) = 1 \rightarrow V(t^+) = 0. \quad (18)$$

Given a constant bias current  $I$  and an initial condition  $V(0) = 0$ , the membrane potential of the cell evolves according to

$$V(t) = I(1 - e^{-t}). \quad (19)$$

If  $I > 1$ , the cell will reach the threshold  $V = 1$ , "spike", reset to  $V = 0$ , evolve again according to equation (19), and repeat this process with a characteristic oscillatory period (see Figure 16(a)). The period  $\Delta T^*$  can be determined by setting  $V(\Delta T^*) = 1$  in equation (19) and solving for  $\Delta T^*$ , yielding

$$\Delta T^* = \ln\left(\frac{I}{I-1}\right). \quad (20)$$

Notice that the period monotonically decreases as the bias current  $I$  is increased.

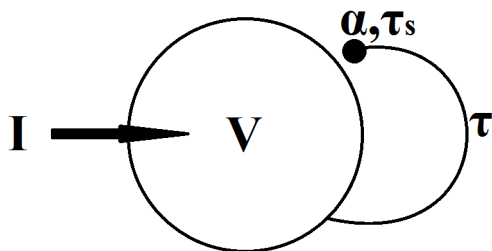


Figure 15: The DSI cell with constant applied current  $I$ , membrane potential (cell voltage)  $V$ , synaptic delay  $\tau$ , synaptic strength  $\alpha$ , and synaptic decay rate  $\tau_s$ .

We now consider an LIF model of a cell with a delayed self-inhibitory synapse (an inhibitory "autapse"), which we refer to as the DSI cell. We assume that when a sufficiently large constant current ( $I > 1$ ) is applied to the resting DSI cell, the cell's membrane potential rises to the firing threshold ( $V = 1$ ), after which it resets and begins to grow again according to the LIF model. However, a self-inhibitory current activates at time  $\tau$  after the cell fires. This delayed self-inhibition is modeled by an exponentially-decaying, non-summing current-based synapse.

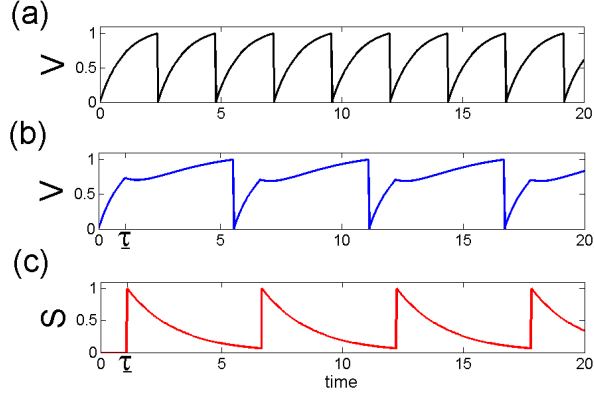


Figure 16: (a) The evolution of the LIF cell’s membrane potential  $V(t)$  for  $I = 1.1$ . (b) The evolution of the DSI cell’s membrane potential  $V(t)$  and (c) synaptic waveform  $S(t - \tau)$  for  $I = 1.1, \alpha = .5, \tau = 1.1, \tau_s = 2$ .

The dynamics of the DSI cell are described by

$$\frac{dV}{dt} = -V + I - \alpha S(t - \tau), \quad (21)$$

$$\frac{dS}{dt} = \frac{-S}{\tau_s}, \quad (22)$$

$$V(t^-) = 1 \rightarrow S(t^+) = 1.$$

$$V(t^+) = 0$$

In equation (21),  $\alpha S(t - \tau)$  is the delayed synaptic current where  $\alpha$  is the nondimensional synaptic strength,  $S(t)$  is the time-dependent synaptic waveform, and  $\tau$  is the fixed delay. In equation (22),  $\tau_s$  is the decay rate of the exponential synapse.

Figure 16(b) illustrates the suppressing effect of the synaptic self-inhibition on the DSI cell’s oscillatory activity as described in equations (21 -22). The peak of the synaptic current corresponds to the activation of the inhibitory autapse and occurs  $\tau$  time after the spike of the DSI membrane potential (see Figure 16(c)). The inhibition suppresses the cell’s voltage and thus lengthens the inter-spike intervals compared to the standard LIF cell (compare Figure 16(a) and (b)). In section II, we show how to compute the period semi-analytically.

## 9 Evolution of the Inter-Spike Interval and the Characteristic Period of the DSI Cell

In order to examine the phase-locking and phase-response properties of the DSI cell, we must first determine the period of the cell’s oscillatory activity and the period’s dependence

on parameter values. This involves a significantly more extensive derivation than the derivation for the period of the LIF model in equation (20). Calculating the period of the DSI cell involves finding a piecewise solution of equations (21-22) for the successive interspike intervals and then combining these solutions to define an interspike-interval (ISI) map. The fixed point of the ISI map corresponds to the period of the DSI cell.

To construct the ISI map, first suppose that the cell spikes and is reset to  $V = 0$  at time  $t = T_{k-1}$ . The inhibitory autapse activates at time  $t = T_{k-1} + \tau$  (point A in Figure 17). We define the cell's voltage at the onset of inhibition to be  $V_k = V(T_{k-1} + \tau)$ .  $V$  evolves according to equation (21) between time  $T_{k-1} + \tau$  and the next firing time  $T_k$ , with the synaptic current decaying exponentially according to equation (22). Therefore we can integrate equation (21) from  $T_{k-1} + \tau$  to  $T_k$  (point A to point B) to obtain

$$V(T_k)e^{T_k} - V_k e^{T_{k-1} + \tau} = I(e^{T_k} - e^{T_{k-1} + \tau}) - \alpha \int_{T_{k-1} + \tau}^{T_k} e^t S(t - \tau) dt. \quad (23)$$

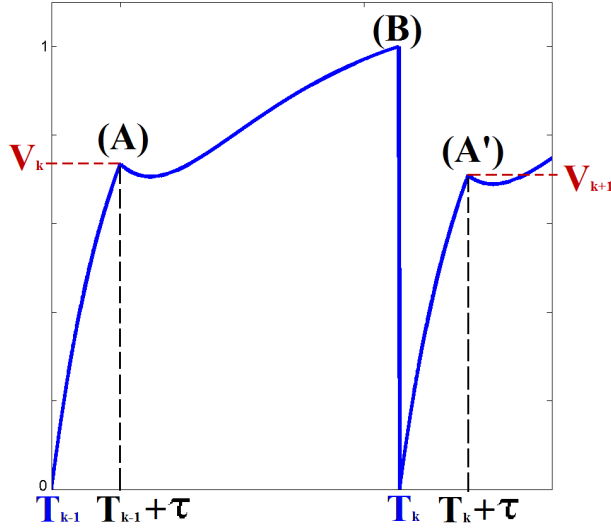


Figure 17: The firing times  $T_i$  (blue) and the voltage values  $V_i = V(T_{i-1} + \tau)$  (red) at the inhibition-activation timings  $T_{i-1} + \tau$  (black).

To find the firing time  $T_k$  and thus the  $k^{th}$  inter-spike interval  $\Delta T_k = T_k - T_{k-1}$ , we set

$V(T_k^-) = 1$  and solve equation (23) for  $V_k$

$$\begin{aligned}
V_k &= e^{\Delta T_k - \tau} - I(e^{\Delta T_k - \tau} - 1) \\
&+ \alpha \frac{\tau_s}{\tau_s - 1} \left( e^{\frac{(\Delta T_k - \tau)(\tau_s - 1)}{\tau_s}} - 1 \right) \\
&= F(\Delta T_k).
\end{aligned} \tag{24}$$

Note that equation (24) gives the ISI  $\Delta T_k$  implicitly in terms of  $V_k$ .

To complete a full cycle of the oscillatory activity of the DSI cell, we must find the cell's voltage when the autapse is next activated, i.e.,  $V_{k+1} = V(T_k + \tau)$  (point A' in Figure 17). We integrate equation (21) from  $T_k$  to  $T_k + \tau$  (point B to point A') with initial condition  $V(T_k^+) = 0$  to obtain

$$\begin{aligned}
V_{k+1} &= I(1 - e^{-\tau}) - \frac{\alpha \tau_s}{\tau_s - 1} e^{\frac{-(\Delta T_k - \tau)}{\tau_s}} \left( e^{\frac{-\tau}{\tau_s}} - e^{-\tau} \right) \\
&= G(\Delta T_k).
\end{aligned} \tag{25}$$

Equation (25) gives the voltage at the time at which the delayed inhibition activates,  $V_{k+1}$ , in terms of the preceding ISI  $\Delta T_k$ . By equating equation (24) in the form  $V_{k+1} = F(\Delta T_{k+1})$  with equation (25), we create a finite-difference equation for successive ISIs, which we call the ISI map

$$F(\Delta T_{k+1}) = G(\Delta T_k). \tag{26}$$

This map takes the  $k^{\text{th}}$  inter-spike interval duration  $\Delta T_k$  as input and outputs the duration of the  $(k + 1)^{\text{th}}$  inter-spike interval  $T_{k+1}$ . It captures the essential dynamics of the repetitively firing DSI cell subject to a constant bias current, and it can be iterated to find the evolution of the inter-spike intervals  $\Delta T_k$ . The fixed point  $F(\Delta T^*) = G(\Delta T^*)$  corresponds to the characteristic period of the DSI cell.

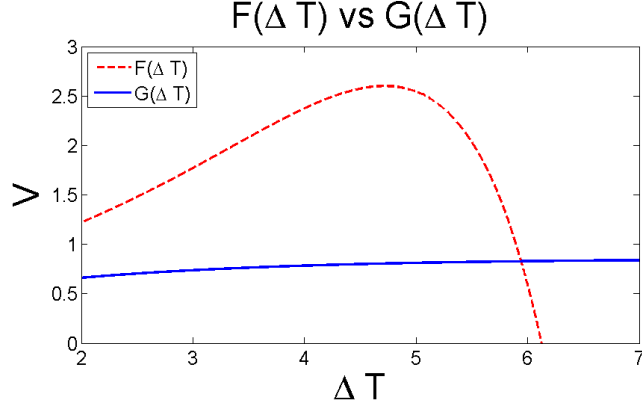


Figure 18: The graphical representation of ISI map (eqn. (26)):  $V_{k+1} = F(\Delta T_{k+1})$  and  $V_{k+1} = G(\Delta T_k)$ . The intersection of  $F$  and  $G$  indicates the fixed point  $\Delta T^* \approx 5.943$ .  $\{I = 1.1, \alpha = .5, \tau = 1.5, \tau_s = 2\}$

Given appropriate initial conditions, the iterates of the map will converge to the fixed point  $\Delta T^*$  if  $|G'(\Delta T^*)/F'(\Delta T^*)| < 1$ , (i.e., the inequality  $|G'(\Delta T^*)| < |F'(\Delta T^*)|$  seen in Figure 18). Figure 18 shows an example of map (26) for the set of parameters  $\{I = 1.1, \alpha = .5, \tau = 1.5, \tau_s = 2\}$ . This case has fixed point  $\Delta T^* \approx 5.943$  and  $|\frac{G'(\Delta T^*)}{F'(\Delta T^*)}| \approx 0.0035 \ll 1$ , indicating that the fixed point is stable and in fact highly attractive.

Over the wide parameter sets that we examined ( $1.01 < I < 1.5, .1 < \alpha < .9, .1 < \tau < 2, .1 < \tau_s < 3$ ), the map always had a unique, stable, and highly attractive fixed point  $\Delta T^*$ . Thus, for all parameter sets, if the DSI cell is slightly perturbed away from the periodically oscillating state (e.g. via an excitatory or inhibitory current), it quickly returns to its stable characteristic period.

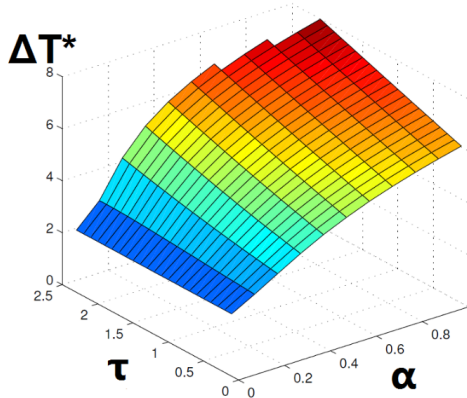


Figure 19: The stable period length  $\Delta T^*$  varies with inhibition-timing  $\tau$  and inhibition-strength  $\alpha$ .  $I = 1.1$ ,  $\tau_s = 2$ .

Figure 19 shows how the period of the DSI cell  $\Delta T^*$  depends on the synaptic delay  $\tau$  and the inhibition strength  $\alpha$ . The stronger the self-inhibition (larger  $\alpha$ ), the longer the period, because the depression will be larger and thus the cell will take longer to reach threshold. Similarly, the slower the self-inhibition decays (larger synaptic decay rate  $\tau_s$ ), the larger the depression and longer the period (not shown). The larger the synaptic delay  $\tau$ , the longer the period.

Note also that the values of  $\Delta T^*$  in Figure 19 at  $\alpha = 0$  (no delayed inhibition) correspond to the characteristic period of the original LIF model,  $\ln(\frac{I}{I-1})$ . As was the case in the standard LIF model, the larger the bias current  $I$ , the faster the cell voltages grow and the shorter the period lengths (not shown).

## 10 The Infinitesimal Phase Response Curve (iPRC)

We are now ready to determine the phase response properties of the DSI cell. Assuming that the DSI cell is oscillating with its intrinsic period  $\Delta T^*$ , we define “phase” as the timing in the periodic firing cycle of the DSI cell, so phase 0 is the beginning of the cycle (at which the voltage is 0), phase  $\tau$  is the phase at which the autapse activates, and phase  $\Delta T^*$  is the firing phase. Note that during steady oscillatory activity the DSI cell is  $\Delta T^*$ -periodic, so phase 0 is equivalent to phase  $\Delta T^*$ .

A brief, small current pulse delivered to the DSI cell at phase  $\Omega/\Delta T^*$  results in an abrupt change in the cell’s membrane potential of  $\Delta V$ . This change in voltage causes a “phase shift” in the DSI cell’s firing cycle, thereby causing the cell to fire at a different time. An example is illustrated in Figure 20 of a negative phase shift, or phase delay. The DSI cell receives an inhibitory stimulus at phase  $\Omega$  that suppresses its voltage by  $\Delta V$  and causes the cell to fire later than its unperturbed time. Specifically on the first cycle after

the perturbation, the cell's ISI is  $\Delta T_0 = \Delta T^* + \Delta\Theta_0$ , where  $\Delta\Theta_0$  is the initial phase shift due to the perturbation.

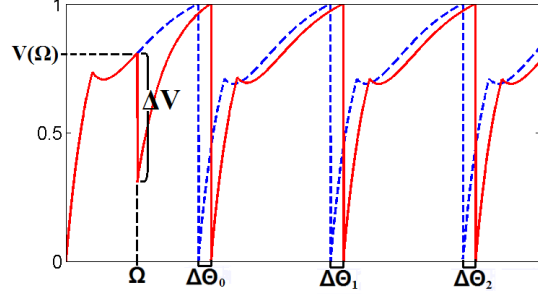


Figure 20: An inhibitory stimulus at time  $\Omega$  (phase  $\Omega/\Delta T^*$ ) suppresses the cell's voltage by  $\Delta V$  and causes a phase delay  $\Delta\Theta_0$ . The solid red curve shows the evolution of the perturbed DSI cell's voltage, while the dashed blue curve shows the unperturbed case. After each cycle, the perturbed cell has a new phase shift  $\Delta\Theta_k$  (relative to the unperturbed cell), which converge to  $\Delta\Theta$  as the cell recovers. Computed with  $\{I = 1.1, \alpha = .5, \tau = 1.1, \tau_s = 2, \Omega = .5, \Delta V = .5\}$ .

Note that the DSI cell does not immediately return to its periodic behavior. On the  $k^{\text{th}}$  cycle, the ISI duration is  $\Delta T_k = \Delta T^* + \Psi_k$ , where  $\Psi_k$  is defined as the additional phase shift. Because the ISIs of the DSI cell quickly converge back to the period  $\Delta T^*$  (i.e.,  $\Delta T_k \rightarrow \Delta T^*$  as  $k \rightarrow \infty$ , see Section III),  $\Psi_k \rightarrow 0$  quickly as well. The cumulative phase shifts of the cell for  $k$  cycles after the perturbation are  $\Delta\Theta_k = \sum_{i=1}^k \Psi_i$ , and  $\Delta\Theta_k \rightarrow \Delta\Theta$ , which is the asymptotic phase shift. The deviation in ISI duration is thus only temporary, but the cell's oscillatory activity remains shifted by phase  $\Delta\Theta$ .

For the DSI cell, we can derive the iPRC semi-analytically. We compute the initial phase shift  $\Delta\Theta_0$  due to a perturbation at phase  $\Omega$ , and then we calculate the lasting phase shift  $\Delta\Theta$  by iterating the ISI map (equation (26)). Measuring  $\Delta\Theta_0(\Omega)$  and calculating  $\Delta\Theta$  for every time  $\Omega$  between times 0 and  $\Delta T^*$  defines the asymptotic phase response curve (PRC).

To determine the initial phase shift  $\Delta\Theta_0(\Omega)$ , we must find the next firing time  $\Delta T_0 = \Delta T^* + \Delta\Theta_0$  after the voltage change  $\Delta V$  at phase  $\Omega$ . The derivation for  $\Delta T_0$ , and therefore the initial phase shift  $\Delta\Theta_0$ , depends on whether or not the perturbation comes before or after the autapse activates:

#### **Finding $\Delta\Theta_0$ for $\Omega < \tau$ :**

The voltage at which the autapse activates following the perturbation  $\Delta V$  at phase  $\Omega$  is  $V(\tau) = V^* + \Delta V e^{-(\tau-\Omega)}$ . By using  $V_0 = V(\tau)$  in equation (24), we can compute the firing time  $\Delta T_0$ . Because the perturbation  $\Delta V$  is small, the initial phase shift  $\Delta\Theta_0$  is small

and we can linearize equation (24) around  $\Delta T^*$ . Thus,  $V_0 = F(\Delta T_0)$  becomes

$$\begin{aligned} V^* + \Delta V e^{-(\tau-\Omega)} &= F(\Delta T^* + \Delta\Theta_0) \\ F(\Delta T^*) + \Delta V e^{-(\tau-\Omega)} &\approx F(\Delta T^*) + \Delta\Theta_0 F'(\Delta T^*). \end{aligned}$$

Solving for  $\Delta\Theta_0$ ,

$$\Delta\Theta_0 \approx -\Delta V e^{-(\tau-\Omega)} \frac{1}{F'(\Delta T^*)}. \quad (27)$$

**Finding  $\Delta\Theta_0$  for  $\Omega > \tau$ :**

We compute the voltage immediately before the cell is stimulated ( $V(\Omega)$  in Figure 20) in a manner similar to the derivation of equations (23-24)

$$\begin{aligned} V(\Omega) &= I(1 - e^{-\Omega+\tau}) + V^* e^{-\Omega+\tau} \\ &\quad - \alpha \frac{\tau_s}{\tau_s - 1} \left( e^{\frac{-\Omega+\tau}{\tau_s}} - e^{-\Omega+\tau} \right). \end{aligned} \quad (28)$$

We then add the voltage change  $\Delta V$  from the perturbation to  $V(\Omega)$ , and use  $V(\Omega) + \Delta V$  as the initial condition with differential equations (21-22) to find the firing time  $\Delta T_0$  (in a manner similar to the derivation of equation (25))

$$\begin{aligned} V(\Delta T_0) &= 1 = I(1 - e^{-\Delta T_0+\Omega}) \\ &\quad + (V(\Omega) + \Delta V) e^{-\Delta T_0+\Omega} \\ &\quad - \alpha \frac{\tau_s}{\tau_s - 1} \left( e^{\frac{-\Delta T_0+\Omega}{\tau_s}} - e^{-\Delta T_0+\Omega} \right). \end{aligned} \quad (29)$$

Equation (29) must be solved numerically for  $\Delta T_0$ . Note that this is the only non-analytical piece of the derivation for the iPRC.

After the initial phase shift  $\Delta\Theta_0$  is computed, the subsequent phase shifts  $\Psi_k$  can be found by iteration of the ISI map (eqn. (26)) using  $\Delta\Theta_0$  as the initial condition. Because the perturbation is small, the phase shifts are small enough that we can linearize the ISI map around the fixed point  $\Delta T^*$  to approximate  $\Psi_k$

$$\begin{aligned} F(\Delta T^* + \Psi_k) &= G(\Delta T^* + \Psi_{k-1}) \\ F(\Delta T^*) + \Psi_k F'(\Delta T^*) &\approx G(\Delta T^*) + \Psi_{k-1} G'(\Delta T^*) \\ \Psi_k &\approx \frac{G'(\Delta T^*)}{F'(\Delta T^*)} \Psi_{k-1}. \end{aligned}$$

The analytical solution to this first-order linear homogenous difference equation with initial condition  $\Psi_0 = \Delta\Theta_0$  is

$$\Psi_k = \left[ \frac{G'(\Delta T^*)}{F'(\Delta T^*)} \right]^k (\Delta\Theta_0). \quad (30)$$

Note that  $\left| \frac{G'(\Delta T^*)}{F'(\Delta T^*)} \right| \ll 1$  for all parameter sets considered (see Section III), so these additional phase shifts  $\Psi_k$  converge very quickly to zero. The accumulative phase shifts  $\Delta\Theta_k = \sum_{i=0}^k \Psi_k$  converge as  $k \rightarrow \infty$  to a value  $\Delta\Theta$ , the asymptotic phase shift. Calculating the initial phase shift  $\Delta\Theta$  for every phase of perturbation  $\Omega$  determines our PRC.

Note that because the voltage change  $\Delta V$  from a perturbation is sufficiently small, the cell's phase response  $\Delta\Theta$  should be proportional to  $\Delta V$ . Normalizing the PRC with respect to  $\Delta V$  yields the infinitesimal PRC (iPRC). The iPRC is also called the phase sensitivity function. Note that the iPRC can be used to determine the quantitative phase response to a perturbation simply by multiplying the amplitude of the stimulus by the magnitude of the PRC at the phase of the perturbation.

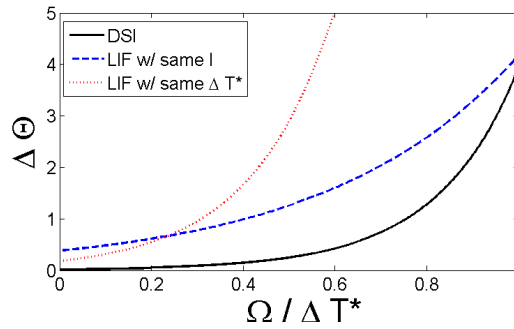


Figure 21: The asymptotic iPRCs for the DSI cell with  $\Delta T^* \approx 5.5708$ ,  $I = 1.1$ ,  $\alpha = .5$ ,  $\tau = 1.5$ ,  $\tau_s = 2$  (solid black), a standard LIF cell with  $\Delta T^* = 2.3979$ ,  $I = 1.1$  (dashed blue), and a standard LIF cell with  $\Delta T^* = 5.5708$ ,  $I = 1.0038$  (dotted red). The dotted red iPRC peaks at  $\Delta\Theta \approx 50$ , so it was cropped to emphasize the smaller differences between the iPRCs.

Figure 21 shows the iPRC for the DSI cell with  $\{I = 1.1, \Delta T^* \approx 5.5708\}$  (solid black), the iPRC for a standard LIF cell with the same bias current  $\{I = 1.1\}$  (dashed blue), and the iPRC for a standard LIF cell with the same period  $\{\Delta T^* = 5.5708\}$  (dotted red). The iPRCs show that the DSI cell has very different phase response properties than the LIF cell. The DSI cell is less sensitive to perturbations for all  $\Omega$  than the standard LIF cell with similar parameters (same bias current  $I$ ), especially at later phases. This decreased sensitivity is even more pronounced when  $I$  is adjusted to equalize the period of the LIF cell to that of the DSI cell. The DSI cell is less sensitive overall to earlier and later perturbations despite having an increased  $\Delta T^*$ , which would typically increase sensitivity of the LIF cell.

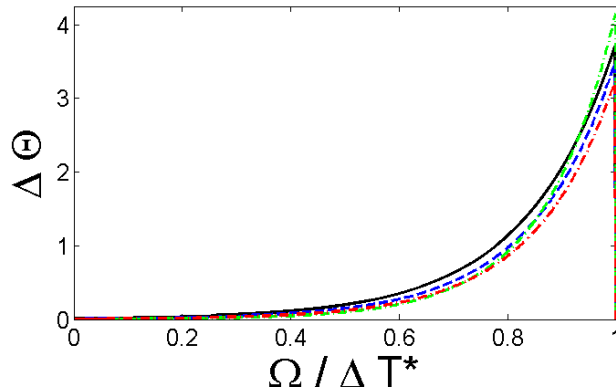


Figure 22: The asymptotic infinitesimal phase response curves show how a stimulus at phase  $\Omega/\Delta T^*$  causes a lasting phase shift  $\Delta\Theta$  in the DSI cell’s oscillatory behavior. The curves are given by  $I = 1.1$  and:  $\alpha = .5, \tau = 1.5, \tau_s = 2$  (solid black);  $\alpha = .5, \tau = 2, \tau_s = 2$  (dashed blue);  $\alpha = .5, \tau = 1.5, \tau_s = 3$  (dot-dashed green);  $\alpha = .7, \tau = 1.5, \tau_s = 2$  (dotted red).

Figure (22) shows iPRCs for the DSI cell with various parameters. Despite quantitative differences between the iPRCs, the shape and qualitative behavior of the iPRCs was largely similar for the parameter sets examined ( $1.01 < I < 1.5$ ,  $.1 < \alpha < .9$ ,  $.1 < \tau < 2$ ,  $.1 < \tau_s \leq 3$ ). Changing the period  $\Delta T^*$  of the DSI cell has a much more nuanced effect on the cell’s sensitivity than in case of the LIF cell. We use the solid black iPRC in Figure 22 as the base case iPRC for comparison. Similar to the LIF cell, increasing  $\Delta T^*$  via an increase in  $\tau_s$  or a decrease in  $I$  (see Section III) decreases the magnitude of the iPRC at early times and increases the magnitude at later times, making the DSI cell less sensitive to early perturbations and more sensitive to later perturbations. The effect of increasing  $\tau_s$  can be seen by comparing the base iPRC to the dot-dashed green iPRC. However, increasing  $\Delta T^*$  via an increase in  $\tau$  or  $\alpha$  (see Section III), decreases the overall magnitude of the iPRC, making the DSI cell less sensitive overall to perturbations. The effect of increasing  $\alpha$  can be seen by comparing the base iPRC to the dotted red iPRC, while the effect of increasing  $\tau$  can be seen by comparing the base iPRC to the dashed blue iPRC. Thus, it is possible to increase  $\Delta T^*$  and get an opposite change in sensitivity for the DSI cell as compared to the standard LIF cell.

## 11 Phase-Locking in DSI Cell Pairs

Using the iPRC obtained in Section IV, we can predict the phase-locking behavior of networks of DSI cells. We consider two DSI cells that are weakly coupled with delayed mutual inhibition via either exponentially-decaying, non-summing current-based synapses (as in the autapse) or  $\delta$ -function synapses, which is the limiting case of fast synaptic decay.

Each cell has membrane potential  $V_i$  and an inhibitory autapse with synaptic delay  $\tau$ , synaptic strength  $\alpha$ , and synaptic decay rate  $\tau_s$ . The coupling is modeled with synaptic delay  $\tau_c$ , synaptic strength  $\varepsilon$ , and synaptic decay rate  $\tau_{sc}$ . Both cells are stimulated with bias current  $I$  to induce oscillations (see Figure 23).

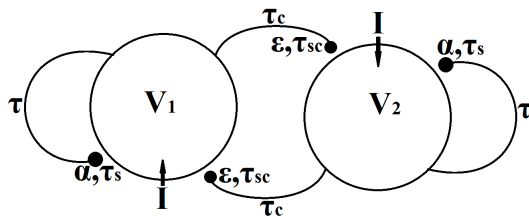


Figure 23: The pair of weakly coupled DSI cells, each with constant applied current  $I$ , membrane potentials  $V_1$  and  $V_2$ , synaptic delays  $\tau$ , synaptic strengths  $\alpha$ , and synaptic decay rates  $\tau_s$ . The connecting synapses have synaptic delays  $\tau_c$ , synaptic strengths  $\varepsilon$ , and synaptic decay rates  $\tau_{sc}$ .

We define  $\Phi_i$  to be the phase of cell  $i$  in its periodic cycle and  $\Delta\Phi = \Phi_2 - \Phi_1$  as the relative phase difference between cells 1 and 2. If the cells begin oscillating periodically at some initial phase difference  $\Delta\Phi_1$ , the leading cell will fire first and its input to the following cell will cause a phase delay in the following cell's behavior, thereby increasing the phase difference. When the following cell fires, its input to the leading cell causes a phase delay in the leading cell's behavior, thereby decreasing the phase difference. Eventually these phase shifts will counteract each other consistently every cycle, and the pair will be locked at a stable phase difference  $\Delta\Phi^*$ , i.e., they will phase-lock their oscillatory activity. Figure 24 shows two examples of this behavior. In Figure 24(a), the synaptic delay  $\tau_c = 0$  (no delay) and the two cells with initial phase difference  $\Delta\Phi_1$  asymptotically approach stable antiphase activity (i.e.,  $\Delta\Phi_k \rightarrow 0.5\Delta T^* = \Delta\Phi^*$  as  $k \rightarrow \infty$ ). Figure 24(b) shows that when the synaptic delay is increased ( $\tau_c = 0.75$ ) the two cells asymptotically approach the stable synchronous activity (i.e.,  $\Delta\Phi_k \rightarrow 0 = \Delta\Phi^*$  as  $k \rightarrow \infty$ ).

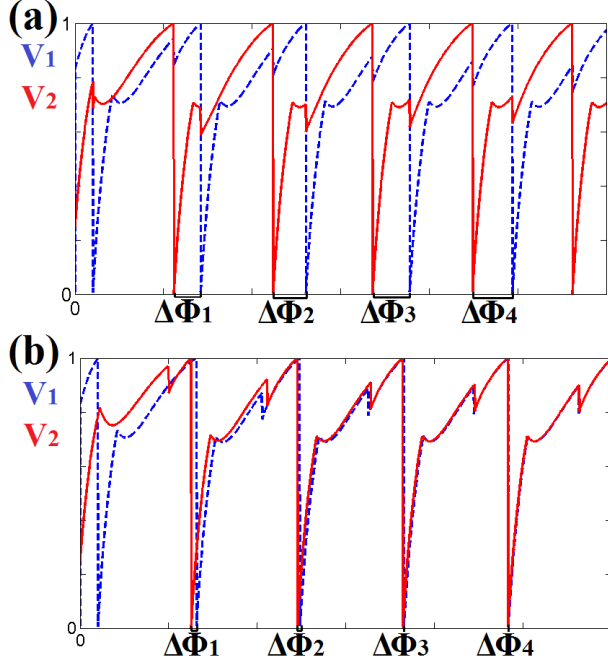


Figure 24: In (a), the pair of weakly coupled DSI cells (with  $\delta$ -function synapses and  $\tau_c = 0$ ) evolves to antiphase phase-locked behavior ( $\Delta\Phi_k \rightarrow 0.5\Delta T^*$  as  $k \rightarrow \infty$ ). In (b), the pair (with  $\tau_c = 0.75\Delta T^*$ ) evolves to synchronous phase-locked behavior ( $\Delta\Phi_k \rightarrow 0$  as  $k \rightarrow \infty$ ). For both cells,  $I = 1.1$ ,  $\alpha = .5$ ,  $\tau = 1.1$ ,  $\tau_s = 2$ ,  $\tau_c = 0.75$ ,  $\varepsilon = .1$ .

We will show how this phase-locking behavior arises analytically, using the iPRC and the theory of weak coupling [?] to derive a single ordinary differential equation for the evolution of phase difference  $\Delta\Phi$  between the two DSI cells and how it depends on parameters.

When uncoupled, cell  $j$  ( $j = 1, 2$ ) undergoes  $\Delta T^*$ -periodic oscillations, and its phase progresses linearly in time, i.e.,  $\Phi_j = t + \Psi_{0j}$ , where  $\Psi_{0j}$  is the initial phase. The instantaneous frequency of the uncoupled cell  $j$  is given by

$$\frac{d\Phi_j}{dt} = 1. \quad (31)$$

Note that the phase difference between the two cells  $\Delta\Phi = \Phi_2 - \Phi_1 = \Psi_{02} - \Psi_{01}$  is constant.

When weakly coupled, the phase of cell  $j$  is defined as  $\Phi_j(t) = t + \Psi_j(t)$ , where  $\Psi_j$  captures the shift in phase due to the coupling, which we call the “relative” phase (with respect to the uncoupled cell). Small synaptic input from cell  $k$  into cell  $j$  slightly increases or decreases the instantaneous frequency, so equation (31) becomes

$$\frac{d\Phi_j}{dt} = 1 + \frac{d\Psi_j}{dt}. \quad (32)$$

At any given time, the adjustment of instantaneous frequency is approximately equal to the product of the input  $\varepsilon S(\Phi_k - \tau_c)$  and the phase sensitivity function  $Z(\Phi_j)$  (the iPRC, see Section IV), and therefore

$$\begin{aligned}\frac{d\Psi_j}{dt} &= Z(\Phi_j)\varepsilon S(\Phi_k - \tau_c) \\ &= \varepsilon Z(t + \Psi_j)S(t + \Psi_k - \tau_c).\end{aligned}\tag{33}$$

$Z$  and  $S$  are both  $\Delta T^*$ -periodic functions, but  $\frac{d\Psi_j}{dt}$  has a timescale of  $\varepsilon$ , which is much slower. Thus the relative phase  $\Psi_j$  of cell  $j$  changes at a slow enough rate that it is essentially constant over a single period  $\Delta T^*$ , and the effect of  $Z$  and  $S$  can simply be averaged over one period. Thus equation (33) becomes

$$\frac{d\Psi_j}{dt} = \frac{\varepsilon}{\Delta T^*} \int_0^{\Delta T^*} Z(t + \Psi_j)S(t + \Psi_k - \tau_c)dt.\tag{34}$$

Subtracting  $\frac{d\Psi_1}{dt}$  from  $\frac{d\Psi_2}{dt}$  (eqn. 34 for  $j = 1, 2$ ) gives the ordinary differential equation for the phase difference  $\Delta\Phi$

$$\begin{aligned}\frac{d\Delta\Phi}{dt} &= H(-\Delta\Phi - \tau_c) - H(\Delta\Phi - \tau_c) \\ &= G(\Delta\Phi; \tau_c).\end{aligned}\tag{35}$$

The zeroes of  $G(\Delta\Phi; \tau_c)$  correspond to phase-locked states for the pair of DSI cells. These phase-locked states  $\Delta\Phi^*$  are stable if  $G'(\Delta\Phi^*; \tau_c) < 0$ , and unstable if  $G'(\Delta\Phi^*; \tau_c) > 0$ . The cell pair will asymptotically approach one of the stable phase-locked states, depending on their initial phase difference. The "attracting region" of a stable state  $\Delta\Phi^*$  corresponds to the set of initial phase differences such that the cell pair will asymptotically approach  $\Delta\Phi^*$ . We are interested in quantifying these phase-locked states and their attracting regions.

For  $\delta$ -function synapses,  $S(t) = \delta(t)$ , and equation (35) simplifies to

$$\frac{d\Delta\Phi}{dt} = \frac{-\varepsilon}{\Delta T^*} (Z(-\Phi + \tau_c) - Z(\Phi + \tau_c)).\tag{36}$$

Figure 25(a) plots equation (36) for  $\tau_c = 0$ . In the system with no intercellular synaptic delay ( $\tau_c = 0$ ), the DSI cell pair evolve to an antiphase state ( $\Delta\Phi^*/\Delta T^* = 0.5$ ). When  $\Delta\Phi/\Delta T^* < 0.5$ ,  $\frac{d\Delta\Phi}{dt} > 0$  and the phase difference grows. When  $\Delta\Phi/\Delta T^* > 0.5$ ,  $\frac{d\Delta\Phi}{dt} < 0$  and the phase difference shrinks. Thus, no matter the initial phase difference (except  $\Delta\Phi_0 = 0$ , the unstable equilibrium), the DSI pair's firing times progress towards antiphase ( $\Delta\Phi^*/\Delta T^* = 0.5$ ).

Including a synaptic delay to the coupling between the two DSI cells changes the zeroes of  $G(\Delta\Phi; \tau_c)$  (eqn. 35) and generates new phase-locked states. This synaptic delay

causes bistability in phase-locking behavior. Depending on the initial phase difference between the two DSI cells, the pair will evolve to either antiphase  $\Delta\Phi^*/\Delta T^* = 0.5$  or synchrony  $\Delta\Phi^*/\Delta T^* = 0$  or  $1$ . Note that since phase is  $\Delta T^*$ -periodic, phases  $0$  and  $\Delta T^*$  are equivalent. In Figure 25, the arrows point towards points that correspond to stable phase-locked states and away from points that correspond to unstable phase-locked states. If the initial phase difference between the two cells is exactly the phase corresponding to the unstable steady states, the cells will remain at that phase difference, but any perturbation to the system will cause the cells to evolve to one of the stable states. In Figure 25(b),  $\tau_c = 0.15\Delta T^*$ , and the attracting region of the antiphase state is larger than that of the synchronous state. In Figure 25(c),  $\tau_c = 0.35\Delta T^*$ , and the opposite is true. In Figure 25(d),  $\tau_c = 0.5$  and the two unstable fixed points have coalesced with the stable fixed point at phase  $\Delta\Phi^*/\Delta T^* = 0.5$ ; thus, with any initial phase difference the cell pair will evolve to synchronous activity ( $\Delta\Phi^*/\Delta T^* = 0$ ). This pattern of growing and shrinking attracting regions of the antiphase and synchronous states repeats periodically as the synaptic delay  $\tau_c$  is increased past  $\Delta T^*$ .

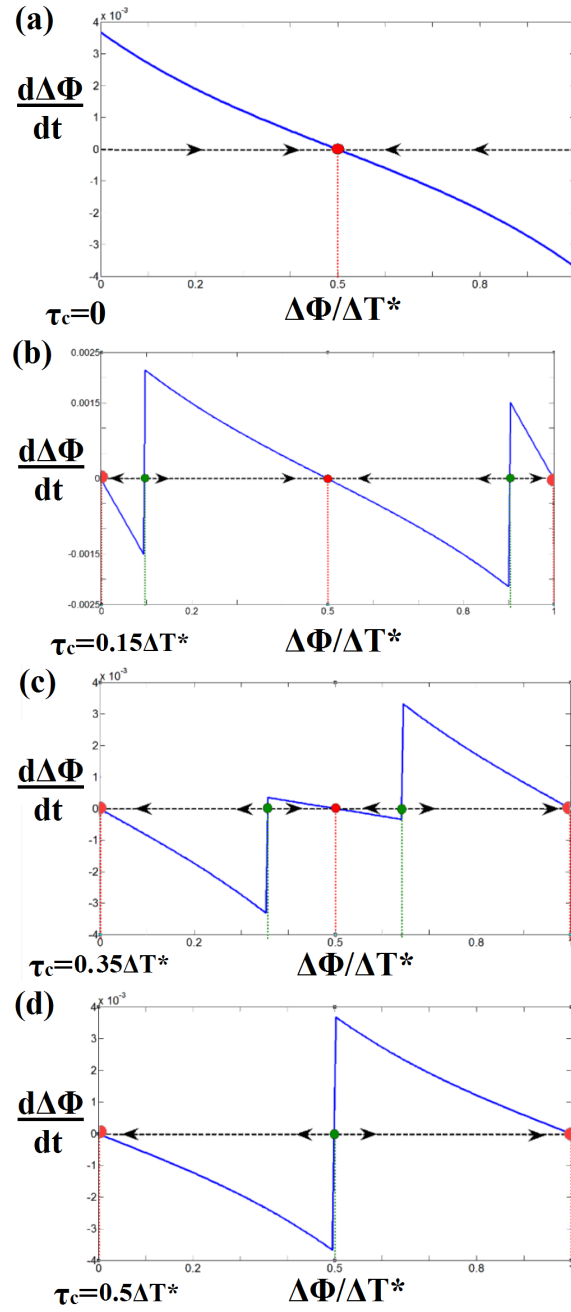


Figure 25: Phase diagrams for DSI cells with  $\delta$ -function synaptic coupling:  $\frac{d\Delta\Phi}{dt}$  vs.  $\Phi$  (eqn. 36) with synaptic delay  $\tau_c$ ,  $\{I = 1.1, \alpha = .5, \tau = 1.1, \tau_s = 2, \varepsilon = .1\}$ .

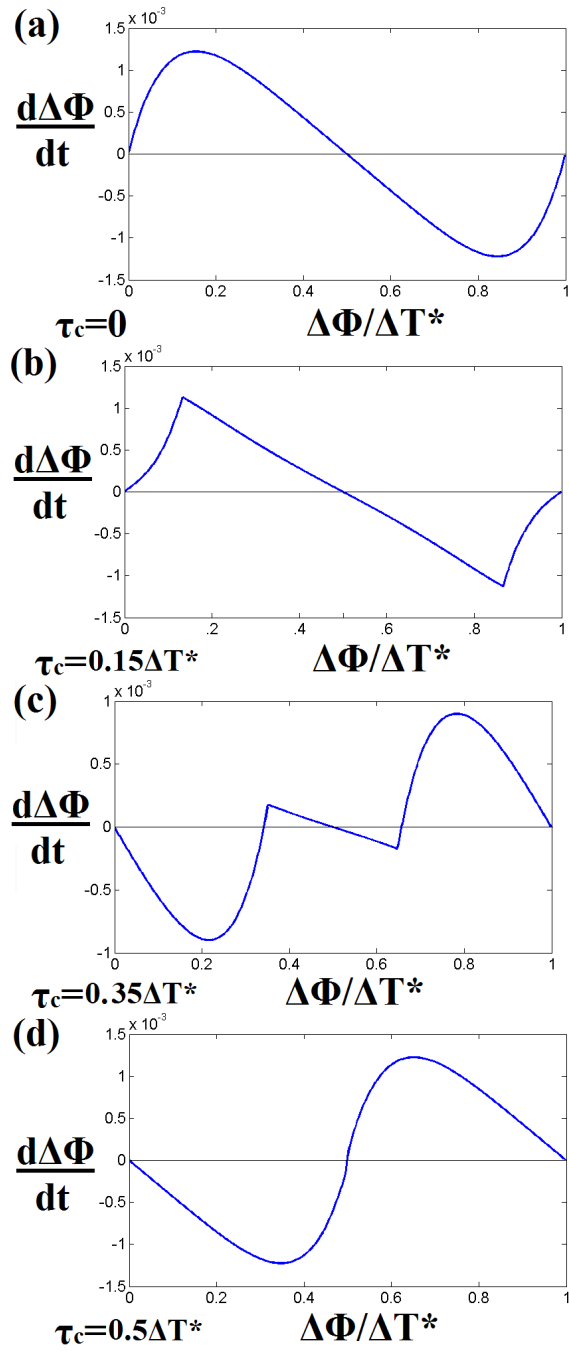


Figure 26: Phase diagrams for DSI cells with exponentially-decaying synaptic coupling:  $\frac{d\Delta\Phi}{dt}$  vs.  $\Phi$  (eqn. 35) with synaptic delay  $\tau_c$ ,  $\{I = 1.1, \alpha = .5, \tau = 1.1, \tau_s = 2, \varepsilon = .1, \tau_{sc} = 100\}$ .

We can summarize these changes in phase-locking behavior as  $\tau_c$  is varied in bifurcation diagrams

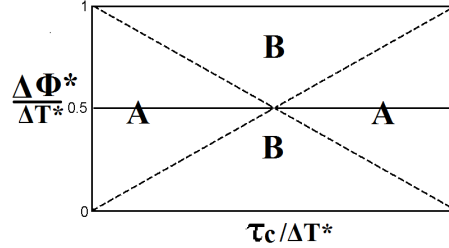


Figure 27: This bifurcation diagram shows the changing stabilities of  $\Phi^*$  for the  $\delta$ -function synaptic coupling as the synaptic delay  $\tau_c$  is varied,  $\{I = 1.1, \alpha = .5, \tau = 1.1, \tau_s = 2, \varepsilon = .1\}$

The bifurcation diagram in Figure 27 summarizes the appearance and disappearance of phase-locked states  $\Phi^*$  as the synaptic delay  $\tau_c$  is varied for the coupled DSI cells with  $\delta$ -function synaptic coupling.

With no delay ( $\tau_c = 0$ ), the only stable phase-locked state is antiphase (synchrony is unstable). As the delay increases, the synchronous state gains stability and a pair of unstable steady states emerge. As the delay approaches phase 0.5, the attracting region B of the synchronous phase-locked state grows and the attracting region A of the antiphase phase-locked state shrinks. At  $\tau_c = 0.5\Delta T^*$ , there is a degenerate pitchfork bifurcation as the unstable states coalesce with the stable antiphase state causing antiphase to go unstable at  $\tau = 0.5\Delta T^*$ , which makes the only stable phase-locked state of this system synchronous. As  $\tau_c$  increases past  $0.5\Delta T^*$ , the antiphase state immediately regains stability and the unstable steady states reemerge. As  $\tau_c$  approaches  $\Delta T^*$ , the attracting region B of the synchronous phase-locked state shrinks and the attracting region A of the antiphase phase-locked state grows. After  $\tau_c = \Delta T^*$ , the pattern of growing and shrinking attracting regions A and B (with a sequence of degenerate pitchfork bifurcations) repeats  $\Delta T^*$ -periodically. For any delay  $\tau_c$  (except  $\tau_c = 0, 0.5\Delta T^*, \Delta T^*, 1.5\Delta T^*, \dots$ ), there is bistability in phase-locking behavior, albeit with unequally-sized attracting regions for the two fixed phase differences.

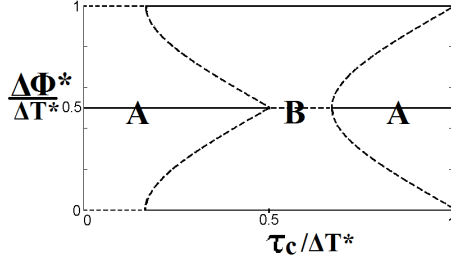


Figure 28: This bifurcation diagram shows the changing stabilities of  $\Phi^*$  for the exponentially-decaying synaptic coupling as the synaptic delay  $\tau_c$  is varied,  $\{I = 1.1, \alpha = .5, \tau = 1.1, \tau_s = 2, \varepsilon = .1, \tau_{sc} = 100\}$

The bifurcation diagram in Figure 28 shows the appearance and disappearance of phase-locked states  $\Phi^*$  as the synaptic delay  $\tau_c$  is varied for the coupled cells with exponentially-decaying synaptic coupling (with decay rate  $\tau_{sc} = 100$ ). There are two important differences between the bifurcation diagrams for the exponentially-decaying synaptic coupling case and the  $\delta$ -function synaptic coupling case (compare Figures 28 and 27). First, the attracting region A of the antiphase phase-locked state does not begin to shrink until  $\tau_c \approx .25\Delta T^*$ . Second, the pitchfork bifurcation is degenerate in the case of  $\delta$ -function synaptic coupling, see Figure 27. At  $\tau_c = 0.5\Delta T^*$ , the unstable states coalesce with the stable antiphase state causing antiphase to go unstable, which makes the only stable phase-locked state of this system synchronous. This remains the only stable phase-locked state until  $\tau_c \approx 0.7\Delta T^*$ . Then antiphase regains stability, and the attracting region B of the synchronous phase-locked state shrinks and the attracting region A of the antiphase phase-locked state grows. After  $\tau_c = \Delta T^*$ , this pattern of shrinking and growing attracting regions A and B (with a sequence of pitchfork bifurcations) repeats periodically. Modeling the synaptic coupling with exponentially-decaying over  $\delta$ -function synapses leads to more robust cases of monostability in phase-locked states.

Altering the individual DSI cell parameters ( $I, \tau, \alpha, \tau_s$ ) changes the iPRCs quantitatively, but does not qualitatively change the phase-locking states of the two-cell system. The general results of this section hold true for any set of parameters that generates an iPRC of the same nature as in the previous section (i.e., for  $1.01 < I < 1.5$ ,  $.1 < \alpha < .9$ ,  $.1 < \tau < 2$ ,  $.1 < \tau_s \leq 3$ ). The parameters that affect the phase-locking are entirely contained in the synaptic connections between the two cells. Increasing the synaptic delay  $\tau_c$  changes the stability of phase-locked antiphase and synchrony and also generates unstable states (see Figures 27-28), while increasing the synaptic decay rate  $\tau_{sc}$  smooths out the dynamics of equation (35) (compare Figures 25 and 26) and quantitatively changes the bifurcation diagram (compare Figure 27 and 28). Changing the synaptic strength  $\varepsilon$  rescales equation (35) but has no effect on the phase-locking states and their stability as long as it remains weak ( $\varepsilon \ll 1$ ).

## 12 Conclusion

In this study, we predict how a neural population with a negative feedback loop oscillates at a characteristic period, responds to perturbations, and synchronizes its oscillatory activity with neighboring groups by using an idealized model of the system, the DSI cell model. The DSI cell's characteristic period arises from cellular and synaptic parameters. Generally, decreasing the bias current or increasing the effects of the "autapse" (via increasing its strength, slowing its decay rate, or timing it later) leads to a longer characteristic period. These parameters also affect the DSI cell's phase sensitivity function (iPRC). Increasing the strength of the autapse or timing the self-inhibition later in the cell's firing cycle leads to an overall decrease in cell's sensitivity, while decreasing the bias current or increasing the decay rate of the autapse typically decreases the sensitivity of the cell to earlier-timed perturbations and increases the sensitivity of the cell to later-timed perturbation.

Mutually-inhibiting DSI cell pairs typically tend to synchronize their firing times in antiphase when there are no synaptic delays, however the presence of synaptic delays can produce in-stable phase activity or bistability between antiphase and in-phase phase-locking states. The cellular and synaptic feedback parameters for the individual DSI cells investigated in the earlier sections have quantitative, but not qualitative, effects on the phase-locking behavior of the pair. Synaptic coupling with slow kinetics (exponentially-decaying synapses) leads to quantitatively different phase-locking behavior than with synapses with faster kinetics ( $\delta$ -function synapses). Specifically, the exponentially-decaying synaptic coupling produces more robust monostability in phase-locking behavior, i.e., there are more synaptic delay values that yield a single stable phase-locked state. Monostability in phase-locked states allows the synchronized oscillations to robustly perform a stable rhythmic role in specific neural networks, whereas bistability in phase-locked states creates neural "switches", where the initial phase difference "switches" the neuron pair to one of the phase-locked states, allowing the system to "remember" input.

The DSI cell has a longer characteristic period and is much less sensitive to weak perturbations than the standard LIF cell with similar parameters. It is far less sensitive than an LIF cell with the same characteristic period, thus the DSI cell model is more than just a standard LIF cell with a longer period. However, the phase-locking behavior of the DSI cell is qualitatively, but not quantitatively, similar to phase-locking in mutually-inhibiting LIF cells (without delayed negative feedback), and it would appear that this qualitative behavior is predominantly determined by the coupling model between the cells. Using a more realistic model of the synaptic coupling between the DSI cells may lead to significant qualitative differences and should be investigated further to determine whether or not the DSI cell model is a good approximation of the behavior of neural systems with delayed negative feedback.

## References

- [1] J.C. Brumberg and B. S. Gutkin. Cortical pyramidal cells as non-linear oscillators: Experiment and spike-generation theory. *Brain Research*, (1171):122–137, 2007.
- [2] G. B. Ermentrout and D. H. Terman. *Mathematical Foundations of Neuroscience*, volume 35 of *Interdisciplinary Applied Mathematics*. Springer, 2010.
- [3] J. Foss, A. Longtin, B. Mensour, and J. Milton. Multistability and delayed recurrent loops. *Physical Review Letters*, 76(4):708–711, February 1965.
- [4] A. L. Hodgkin and A. F. Huxley. A quantitative description of membrane current and its application to conduction and excitation in nerve. *The Journal of Physiology*, 117(4):500–544, 1952.
- [5] F.C. Hoppensteadt and E.M. Izhikevich. *Weakly Connected Neural Networks*. Number v. 126 in Applied Mathematical Sciences. Springer New York, 1997.
- [6] C. L. Johnson. Phase response properties and phase-locking in neural systems with delayed negative feedback. *Explorations - UC Davis Undergraduate Research Journal*, 2015.
- [7] B. Katz and R. Miledi. The measurement of synaptic delay, and the time course of acetylcholine release at the neuromuscular junction. *Proceedings of the Royal Society of London. Series B. Biological Sciences*, 161(985):483–495, February 1965.
- [8] L. Melloni, C. Molina, M. Pena, D. Torres, W. Singer, and E. Rodriguez. Synchronization of neural activity across cortical areas correlates with conscious perception. *The Journal of Neuroscience*, 27:2858–2865, 2007.
- [9] R. Miller. *Oscillatory Event-Related Brain Dynamics*, volume 271 of *NATO ASI Series*, chapter What is the contribution of axonal conduction delay to temporal structure in brain dynamics?, pages 53–57. Springer US, 1994.
- [10] C. Morris and H. Lecar. Voltage oscillations in the barnacle giant muscle fiber. *Journal of Biophysics*, 35:193–213, 1981.
- [11] A. Engel P. Konig and W. Singer. Relation between oscillatory activity and long range synchronization in cat visual cortex. *Proceedings of the National Academy of Sciences of the United States of America*, 92:290–294, 1995.
- [12] M. A. Schwemmer and T. J. Lewis. The theory of weakly coupled oscillators. In R. J. Butera N.W. Schultheiss, A. Prinz, editor, *PRCs in Neuroscience: Theory, Experiment, and Analysis*, volume 6 of *Springer Series in Computational Neuroscience*, pages 3–31. Springer, 2012.

- [13] S. H. Strogatz and I. Stewart. Coupled oscillators and biological synchronization. *Scientific American*, pages 102–109, December 1993.
- [14] S.H. Strogatz. *Sync: How Order Emerges from Chaos In the Universe, Nature, and Daily Life*. Hachette Books, 2012.
- [15] C. Zhang and T. J. Lewis. Phase response properties of half-center oscillators. *Journal of Computational Neuroscience*, 35:55–74, 2013.